ISPRS Journal of Photogrammetry and Remote Sensing 188 (2022) 89–108

Contents lists available at ScienceDirect

ISPRS Journal of Photogrammetry and Remote Sensing

journal homepage: www.elsevier.com/locate/isprsjprs

Cloud and cloud shadow detection for optical satellite imagery: Features, algorithms, validation, and prospects

Zhiwei Li [a], Huanfeng Shen [a,*], Qihao Weng [b], Yuzhuo Zhang [a], Peng Dou [c], Liangpei Zhang [d]

[a] School of Resource and Environmental Sciences, Wuhan University, Wuhan, China
[b] Department of Land Surveying and Geo-Informatics, The Hong Kong Polytechnic University, Hung Hom, Kowloon, Hong Kong
[c] Northwest Institute of Eco-Environment and Resources, Chinese Academy of Sciences, Lanzhou, China
[d] State Key Laboratory of Information Engineering in Surveying, Mapping and Remote Sensing, Wuhan University, Wuhan, China

ARTICLE INFO

Keywords:
Cloud detection
Cloud shadow detection
Optical remote sensing
Satellite imagery
Cloudy and rainy regions

ABSTRACT

The presence of clouds prevents optical satellite imaging systems from obtaining useful Earth observation information and negatively affects the processing and application of optical satellite images. Therefore, the detection of clouds and their accompanying shadows is an essential step in preprocessing optical satellite images and has emerged as a popular research topic in recent decades due to the interest in image time series analysis and remote sensing data mining. This review first analyzes the trends of the field, summarizes the progress and achievements in the cloud and cloud shadow detection methods in terms of features, algorithms, and validation of results, and then discusses existing problems, and provides our prospects at the end. We aim at identifying the emerging research trends and opportunities, while providing guidance for selecting the most suitable methods for coping with cloud contaminated problems faced by optical satellite images, an extremely important issue for remote sensing of cloudy and rainy areas. In the future, expected improvements in accuracy and generalizability, the combination of physical models and deep learning, as well as artificial intelligence and online big data processing platforms will be able to further promote processing efficiency and facilitate applications of image time series. In addition, this review collects the latest open-source tools and datasets for cloud and cloud shadow detection and launches an online project (Open Satellite Image Cloud Detection Resources, i.e., OpenSICDR) to share the latest research outputs (https://github.com/dr-lizhiwei/OpenSICDR).

1. Introduction

The continuous advancement of satellite Earth observation projects in various countries (Harris and Olby, 2001; Neeck et al., 2005; Bézy et al., 2007; Shimada, 2014; Gu and Tong, 2015; Guo et al., 2018) has increased the number of remote sensing satellites at orbit, which can provide massive amounts of data for continuous observations of the Earth's surface. However, as an important source of data for satellite Earth observations, optical satellite images are inevitably contaminated by clouds due to the physical limitations of sensor imaging systems. The International Satellite Cloud Climatology Project estimates a global average annual cloud fraction of up to 66% (Zhang et al., 2004), therefore, the impacts of cloud coverage cannot be overlooked. The presence of clouds impedes optical satellites from acquiring useful information of the Earth's surface and affects the usability of images in different degrees. In addition, shadows projected by clouds on the ground surface also contaminate images. The missing information in images caused by clouds and their shadows leads to spatial and temporal gaps in satellite Earth observation data (Shen et al., 2015) and may cause biases in the subsequent processing and application of images, such as land cover/use change monitoring (Zhu and Woodcock, 2014a), atmospheric variables estimation (Ma et al., 2021), ocean parameters retrieval (Fernandez-Moran et al., 2021).

Cloud and cloud shadow (CCS) detection is an essential step in the preprocessing of optical satellite images. Cloud fraction is an important indicator in image metadata items that can be assessed through cloud detection and are often used as the basis for data availability. Cloud cover assessment filters useful data based on the cloud coverage of images, thereby improving the efficiency of image data storage and transmission (Ghassemi and Magli, 2019; Giuffrida et al., 2020). In addition, cloud masks are important products of pre-processing optical satellite images that can help maximize the use of the remaining cloud-

* Corresponding author.
E-mail address: shenhf@whu.edu.cn (H. Shen).

https://doi.org/10.1016/j.isprsjprs.2022.03.020
Received 31 December 2021; Received in revised form 23 March 2022; Accepted 31 March 2022
Available online 14 April 2022

free areas in the image and foster image applicability, especially in cloudy and rainy areas (Li et al., 2019a; Zhang et al., 2021d). However, given the common deficiencies of official cloud masks regarding thin cloud omission and false detection of bright surfaces, and the fact that only a few images have associated cloud masks (e.g., Landsat quality assessment band and MODIS cloud mask products), the improvement and development of new CCS detection methods are crucial for the subsequent processing and accurate application of optical satellite images.

Over the past decades, with the release of massive amounts of optical satellite data and the continuous introduction of new data sources, many studies have focused on CCS detection for images taken by different sensors, and many CCS detection methods have been developed. Although the CCS detection literature has been reviewed in previous studies, they mainly focus on the categorization of methodologies (Goodman and Henderson-Sellers, 1988; Zhu et al., 2019a), cloud measuring equipment (Tapakis and Charalambides, 2013), and forms of CCS detection results (Mahajan and Fataniya, 2020). To further conduct a systematic summary of the current achievements and challenges in this field, this study comprehensively reviews the CCS detection literature from the features, algorithms, and validation perspectives as shown in Fig. 1. Different CCS detection methods are reviewed separately from both the features and algorithms perspectives given that algorithms of different categories may achieve CCS detection by using the same type of features and because algorithms of the same category may also accept different types of features. This review also summarizes the main types of CCS detection results and their validation.

On the basis of the involved features, CCS detection algorithms can be categorized as methods based on spectral features, spectral-spatial features, spectral-temporal features, spectral-spatial–temporal features, and multi-source features, which can be extracted from mono-temporal, multi-temporal, and multi-source data. From the perspective of the algorithm, these methods can be roughly classified into physical-rule based, temporal-change based, variational-model based, and machine-learning based algorithms. In addition, CCS detection algorithms usually can be validated by comparing to manually labeled masks, cloud mask products, collocated LiDAR/radar data, or ground-based camera data.

The rest contents are organized as follows. Section 2 conducts the literature analysis. Sections 3 to 5 review the CSS detection from the perspectives of features, algorithms, and validation. Section 6 highlights the problems and prospects in the field. Section 7 concludes the paper.

2. Literature analysis

We have conducted a literature survey with *Scopus* (www.scopus.com) on the topic of cloud and cloud shadow detection for optical satellite imagery, and the search keywords include *cloud/cloud shadow AND detection/masking/extraction/screening/identification*, which are limited to title, keywords, and abstract of the journal articles in English. Based on search results as of December 1, 2021, a total of 1425 journal papers were returned from the *Scopus* database. Eventually, there are 504 papers selected for the literature analysis after manually excluding irrelevant articles. Noted that articles related to cloud classification which further classify clouds into different types according to cloud phase and altitude are not discussed and included in the literature survey. Besides, to ensure the high quality of the papers used for literature analysis, only articles published in formal journals were selected, and each paper was manually checked and confirmed to make sure that it fits the topic of this review. As shown in Fig. 2, the survey result suggests that there is a general increasing trend in the number of published papers and their citations over the past 37 years from 1985 to 2021, especially in the latest decade, which indicates extensive attention was paid to this field recently.

The major countries/region in the field are also listed in Fig. 3 according to the number of published papers (>10), which suggest that the United States, China, and Europe are the three countries/regions that contribute most papers in the field. Besides, considerable research in the field has been conducted in Japan, Canada, India, and Australia. Furthermore, the major institutions which contribute to > 10 papers are also selected and listed in Fig. 4, the results suggest that the top ten institutions are all from China and the United States, among them the Chinese Academy of Science (CAS) and National Aeronautics and Space Administration (NASA) are the two represent institutions of China and the United States that contribute to the most papers in the field, respectively. The only European institution with more than ten papers in the field is the University of Valencia from Spain. Besides, the major journals published most papers (>10) in the field are listed in Fig. 5, in which the top ten journals are selected according to the total number of published papers. The three journals published most papers are *Remote Sensing*, *Remote Sensing of Environment*, and *International Journal of Remote Sensing*, each with >50 articles in the field.

Moreover, the number of papers with different types of satellite images was counted to determine the major types of images that occurred in these 504 papers. The top twelve types of images occurring in >10 papers are selected and shown in Fig. 6, which are sorted by the number of papers that are selected and counted according to whether the satellite keyword occurs in the title, keywords, and abstract of the paper. Fig. 6 also shows the distributions of the number of papers relevant to each type of image over the past each 5–6 years periods from 1985 to 2021. The results indicated that MODIS, Landsat, and AVHRR that are all from the United States are the three types of images that are most widely used for study in the field over the entire period, benefiting from the open data policy (Wulder and Coops, 2014; Harris and

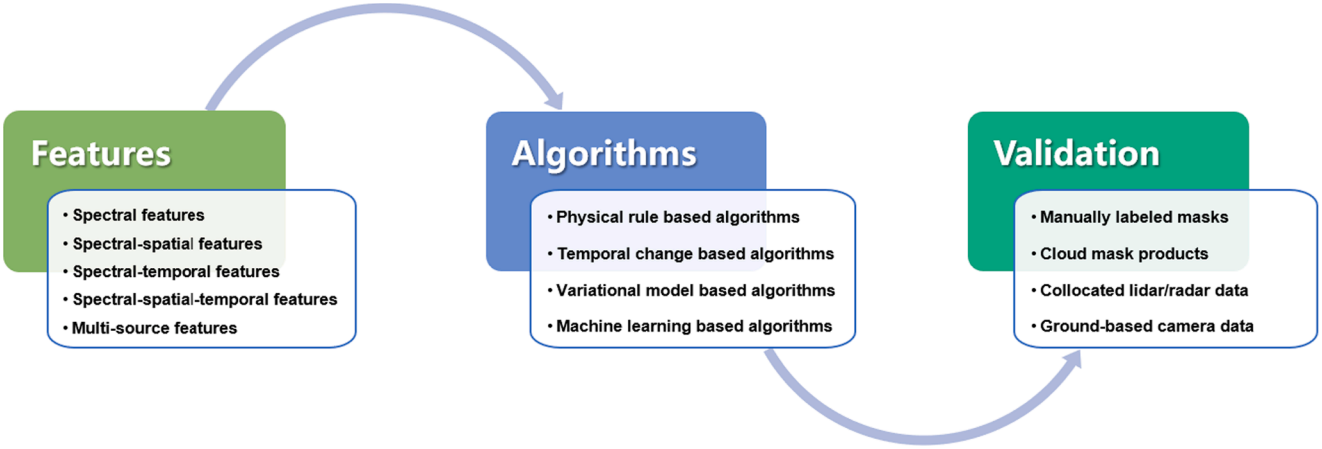

Fig. 1. CCS detection in terms of features, algorithms, and validation.

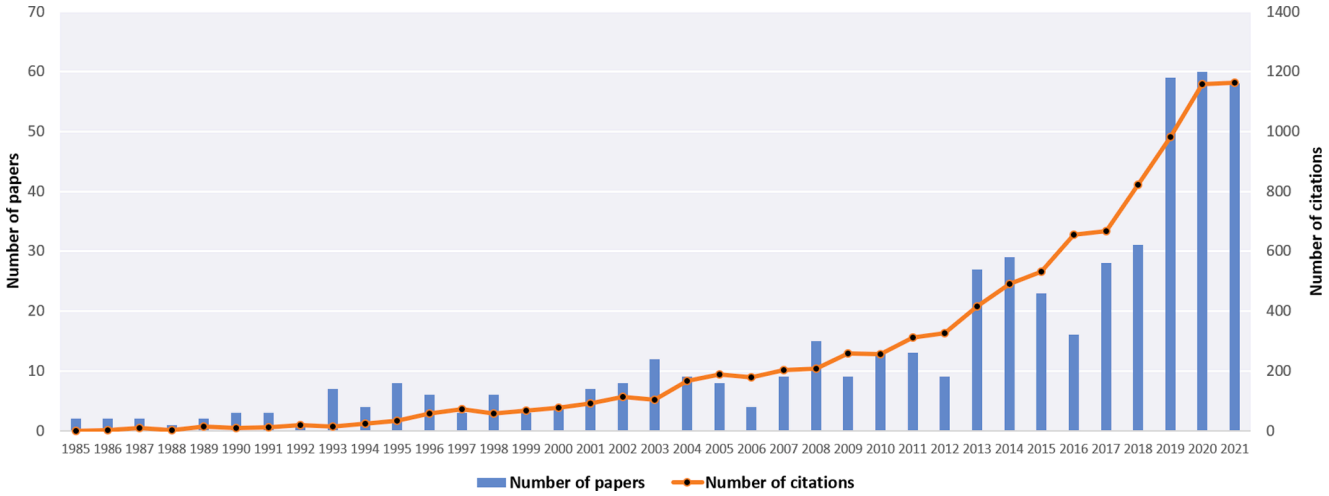

Fig. 2. The number of papers and citations on cloud and cloud shadow detection, 1985–2021.

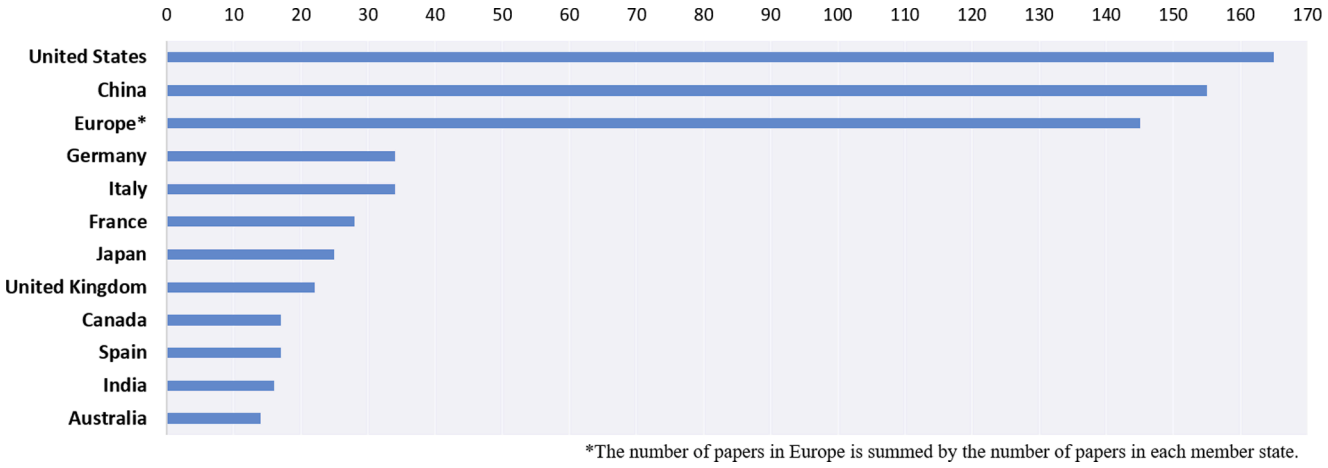

Fig. 3. Major countries/regions (published > 10 journal papers) in the field.

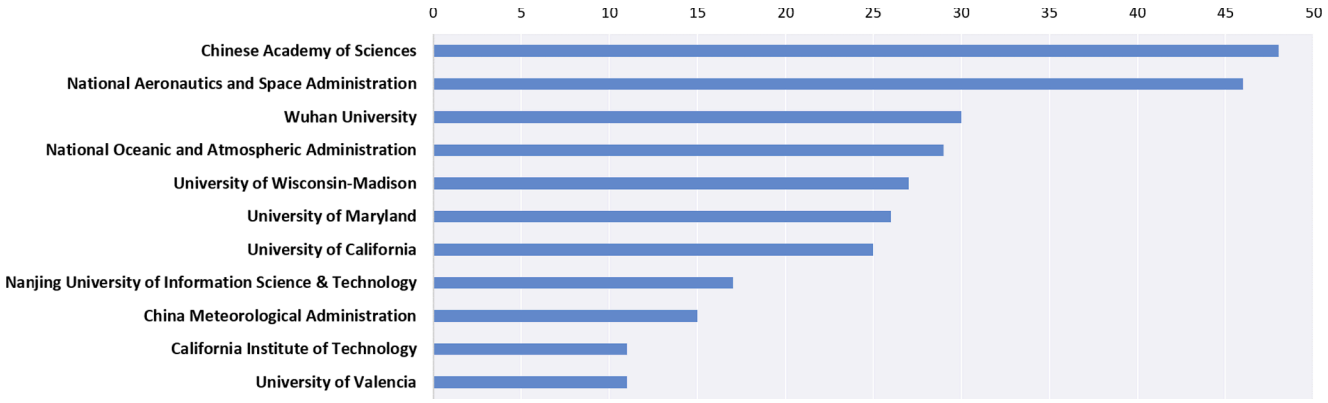

Fig. 4. Major institutions (published > 10 journal papers) in the world.

Baumann, 2015; Zhu et al., 2019b), among them MODIS and Landsat series images are still extensively used as the study data in the recent decade. In addition, the images of the Sentinel from Europe, VIIRS from the United States, Gaofen and Funyun from China, and Himawari from Japan are also been heavily used especially over the latest years from 2016 to 2021, among them the images derived from Chinese Gaofen and Japanese Himawari satellites which are launched in the latest decade have been widely used in recent studies.

3. Features

Depending on the source of input data and the temporal number of images involved, the input for CCS detection may include mono-temporal, multi-temporal, or multi-source data. In this review, it is considered that features can be extracted from spectral, spatial, and temporal domains of images. The typical characteristics of cloud/cloud shadow from different domains are summarized in Table 1, according to

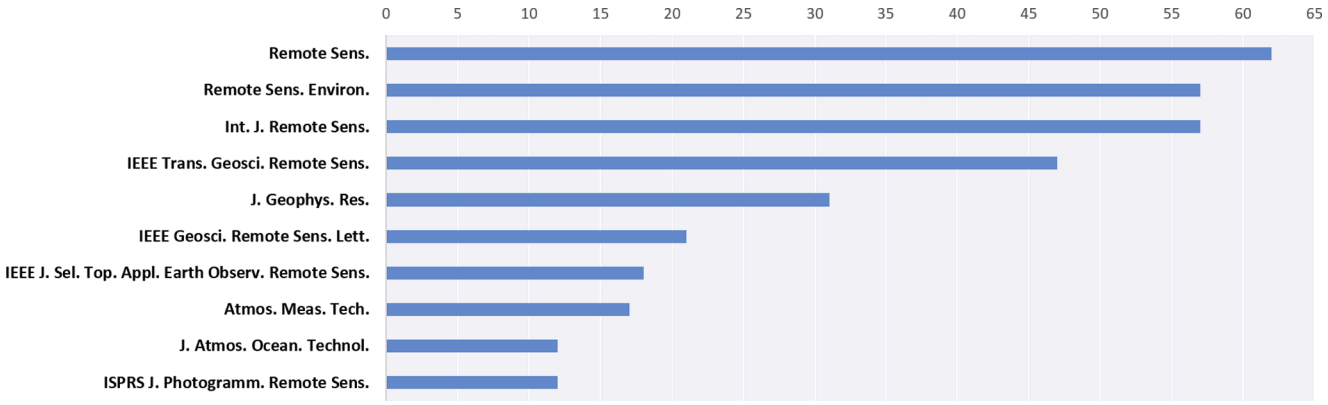

Fig. 5. Major journals (published > 10 journal papers) in the field.

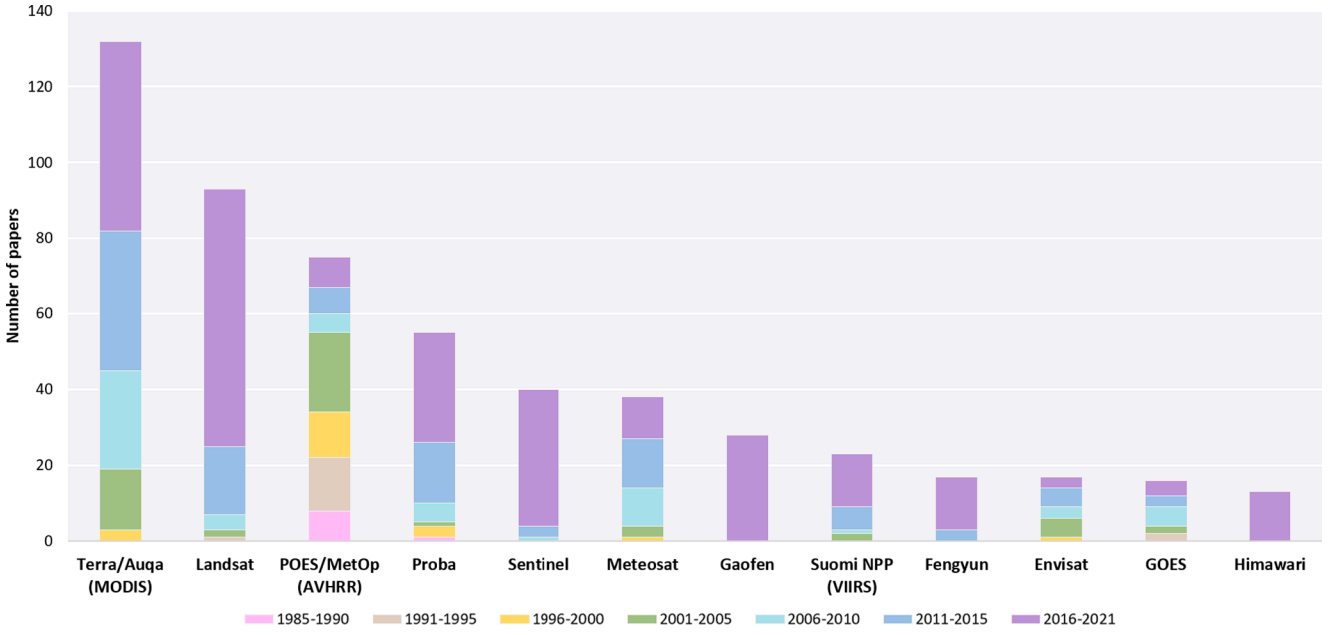

Fig. 6. Major types of satellite images over different periods in the field.

Table 1
Typical characteristics of clouds and cloud shadows from different domains.

Characteristics	Clouds	Cloud shadows
Spectral domain	High brightness White color Low temperature High elevation	Low brightness Dark color
Spatial domain	Spatially smoothing Weak edge Relatively low complexity in shape Sparsity in distribution Spatially adjacent to cloud shadow Similar in shape to cloud shadow	Spatially smoothing Weak edge Relatively low complexity in shape Sparsity in distribution Spatially adjacent to cloud Similar in shape to cloud
Temporal domain	A sharp increase in reflectance	A sharp decrease in reflectance

which features from different domains can be designed and extracted for CCS detection.

Further, according to the domain of features used for CSS detection, CCS detection methods can be classified into spectral-feature based and spectral-spatial-feature based methods for mono-temporal images, spectral-temporal-feature based and spectral-spatial–temporal-feature based methods for multi-temporal images. Besides, multi-source features derived from multi-source data are also investigated. Specifically, mono-temporal CCS detection methods are commonly used in practical applications and mainly distinguish cloud/cloud shadow from clear surfaces according to their physical spectral properties or based on multiple types of discriminative spectral and spatial domain features extracted from a single image. Multi-temporal based methods detect CCS by comparing the reflectance differences between the cloud-covered image and the selected cloud-free or predicted clear-sky reference image given that the occurrence of clouds and cloud shadows will lead to abrupt reflectance changes in image time series (Rossow and Garder, 1993; Jedlovec et al., 2008; Goodwin et al., 2013).

3.1. Spectral features

Spectral-feature based methods are usually constructed based on the distinctive spectral features of clouds and cloud shadows as shown in Table 1. These methods artificially and empirically design feature extraction and combine multiple physical spectral rules to perform a threshold segmentation of clouds and shadows (Wang and Shi, 2006; Luo et al., 2008; Sun et al., 2017). The suitable fixed or dynamic

thresholds can be determined through a parametric sensitivity analysis or be defined with the aid of ancillary data (Derrien and Le Gléau, 2005; Ricciardelli et al., 2008). After obtaining a cloud and shadow mask separately, cloud shadows are usually extracted by matching clouds and cloud shadows based on their spatial proximity and geometric similarity.

Spectral-feature based methods are widely used in CCS detection. For example, the automatic cloud cover assessment (ACCA) algorithm (Irish et al. 2006) proposed by the US Geological Survey is used to assess cloud fractions in Landsat-7 images. ACCA contains 26 determination conditions based on physical spectral rules that can effectively detect thick clouds in the images and has been used as the official cloud detection method for supporting image quality assessment. A new method called Fmask (function of mask) (Zhu and Woodcock, 2012; Zhu et al., 2015) was subsequently introduced for the further screening of thin clouds and cloud shadows in Landsat images. Fmask initially builds several spectral rules to extract potential cloud areas then calculates the cloud probabilities based on the spectral variability and brightness temperature for a dynamic-threshold based segmentation of cloud regions to generate cloud masks. Cloud and shadow matching is eventually performed to extract cloud shadows from the image. Given its good performances in different global validation regions, Fmask has been utilized to assess the quality of Landsat 4–8 images. The haze optimized transformation index (HOT) (Zhang et al., 2002, 2014) is proposed to highlight clouds from clear surfaces and has since been simplified and widely used in cloud detection methods (Zhu and Woodcock, 2012; Li et al., 2017; Zhu and Helmer, 2018). The HOT index uses the spectral spaces of blue and red bands to construct a clear line that separates clouds from clear surface pixels, where samples need to be manually selected to determine the optimal transformation coefficients. In addition, the cloud displacement index (CDI) (Frantz et al., 2018), which is designed based on the perspective differences in the three near-infrared bands of Sentinel-2 images, has been proposed to further distinguish cloud and high-bright surfaces and has been integrated into the latest version of Fmask (Qiu et al., 2019).

Although spectral-feature based methods are most commonly used in CCS detection, some physical spectral rules need to be artificially designed to further distinguish cloud/shadow from non-cloud/non-shadow surfaces according to the band setting of a particular image. Afterwards, the statistical analysis is usually performed to determine the optimal segmentation thresholds. However, the selection of rules or thresholds mainly depends on manual empirical judgment and parameter sensitivity analysis, which may involve local biases. In addition, spectral-feature based methods cannot easily cope with complex surfaces due to the phenomenon of homospectral foreign matter (Purkis and Klemas, 2013), and the limited number of extracted spectral features.

3.2. Spectral-spatial features

While spectral-feature based methods only utilize the features of each pixel from the spectral domain, spectral-spatial-feature based methods further mine the spatial features to enhance feature diversity and improve CCS detection performance on complex surfaces of an image.

For example, Li et al. (2017) proposed a multi-feature combined (MFC) method to alleviate the problems of bright surface commission and thin cloud omission in images with limited spectral information. MFC combines spectral, geometric, and texture features for a progressive refinement detection of clouds and shadows. MFC was validated on the global regions and is considered a benchmark for CCS detection in Gaofen-1 WFV images. Moreover, as complements to spectral features, multiple artificially designed spatial features, including edge, geometric, and texture features, have been used in several studies (Lu, 2007; Hu et al., 2015; Bai et al., 2016; Huang et al., 2018; Deng et al., 2019) to increase feature diversity and improve the performance of CCS detection methods. Generally, the combination of spatial features is beneficial for improving CCS detection accuracy, especially for images that only contain visible and near-infrared bands. Meanwhile, high-level spatial features extracted by deep models further enrich the number and variety of features, which can significantly promote the performance of spectral-spatial-feature based methods in CCS detection. In this regard, many deep learning (DL) based CCS detection methods that are based on convolutional neural networks (CNN) (Chen et al., 2020b; Li et al., 2019b, 2021; Wu and Shi, 2018; Xie et al., 2017; Yang et al., 2019) and generative adversarial networks (GAN) (Zou et al., 2019; Mateo-Garcia et al., 2020; Wu et al., 2020), have been developed and demonstrated higher accuracy than threshold based methods that extract only a limited number of features, especially in areas with complex surfaces.

In spectral-feature and spectral-spatial-feature based methods, the extraction of cloud shadow is typically followed by cloud detection (Luo et al., 2008; Zhu and Woodcock, 2012; Braaten et al., 2015). The shadows in optical satellite images broadly include terrain and cloud shadows. Terrain shadows are caused by surface relief, such as mountain and building shadows, which can be removed via topographic correction in combination with DEM and solar incidence angle (Meyer et al., 1993). The locations of cloud shadows in an image are determined by the height of clouds and their location in an image and the angles of the satellite and sun. Therefore, if these parameters are known, then the location of cloud shadows in an image can be approximately predicted by modeling the geometric spatial relationship among the cloud, cloud shadow, sun, and satellite (Simpson and Stitt, 1998; Simpson et al., 2000). However, the height information of clouds in images is difficult to obtain directly, and traditional cloud shadow detection methods identify potential cloud shadow candidates based on the statistical range of the height of most clouds between 200 m and 12 km and on the geometric similarity between clouds and cloud shadows (Luo et al., 2008). After the potential shadow regions are determined, cloud shadows can be isolated within the shadow candidate region by iteratively matching clouds and their shadows over the height range of clouds.

3.3. Spectral-temporal features

The spectral-temporal-feature based methods are mainly based on the spectra of individual pixels and their temporal variations. Such types of methods usually treat CCS detection as a change detection problem. Specifically, pixels in time series with a sudden increase in reflectance are more likely to be clouds, and those pixels with a sudden decrease in reflectance are likely to be cloud shadows.

For example, Hagolle et al. (2010) proposed the multi-temporal cloud detection (MTCD) method, which detects the steep reflectance increase with the blue band and combines the correlation test of neighborhood pixels in multi-temporal images to achieve cloud detection. Results show that MTCD has a stronger ability to discriminate clouds compared with methods that are based on either reflectance or reflectance ratio. Zhu and Woodcock (2014b) proposed the multi-Temporal mask (Tmask) method for CCS detection in multi-temporal Landsat images. Tmask initially applies the Fmask method to produce the initial CCS masks based on each image, models the surface changes based on multi-temporal reflectance data, and further improves CCS mask by comparing the reflectance differences between the model predictions and actual observations. The CSS detection results of Tmask show significant improvements over those of the mono-temporal Fmask method. Lin et al. (2015) developed a multi-temporal cloud detection method based on invariant pixels that extracts the invariant pixel from multi-temporal images via weighted principal component analysis, normalizes multi-temporal images, generates a clear-sky reference image of an image covered by clouds based on invariant pixels in weighted form, and achieves cloud detection by detecting a large difference between the generated cloud-free reference image and the cloud-covered image. Bian et al. (2016) proposed a cloud and snow detection method for multi-temporal Huanjing-1A/1B CCD images that

utilizes 30-day image time series to composite a clean reference image then extract clouds and snow based on the reflectance difference of blue band between the composited reference image and cloud-covered image. Results show that multitemporal information helps improve cloud and snow detection accuracy. Gómez-Chova et al. (2017) performed nonlinear kernel ridge regression based on selected multiple cloud-free images to synthesize the clear-sky reference images of the target date, applied cluster analysis on the differential images of cloud-covered images and clear-sky reference images, determined whether each cluster is a cloud region, and eventually achieved highly accurate multi-temporal cloud detection.

In general, multi-temporal based CCS detection methods usually outperform mono-temporal based methods (Cayula and Cornillon, 1996; Ricciardelli et al., 2008; Zhu and Woodcock, 2014b). Benefiting from the use of multi-temporal information, multi-temporal based methods can alleviate the common problems of thin cloud omission and high-bright objects commission. However, the use of such methods is usually complex and requires the selection of a clear-sky reference image or the construction of a clear-sky reference image by using multi-temporal images over a short period, which may generate errors in areas with rapid and significant land cover changes. Therefore, such types of methods are only suitable for areas with small or periodic land cover changes and images with a high temporal resolution.

3.4. Spectral-spatial-temporal features

Most of the currently available multi-temporal based CCS detection methods only utilize spectral and temporal features based on individual pixels (Hagolle et al., 2010; Bian et al., 2016), hence leaving room for further improving their accuracy by applying methods that utilize spectral, spatial, and temporal domain features simultaneously, especially in areas with complex land cover.

For example, Ricciardelli et al. (2008) developed the cloud MAsk Coupling of Statistical and Physical method (MACSP) algorithm for cloud detection in MSG SEVIRI images, MACSP coupled physical and statistical methods, performed temporal sequence analysis based on the spectral and texture features of multitemporal images, and achieved a good performance when validated against the MODIS cloud mask. Tuia et al. (2018) deployed a recurrent neural network to extract spectral-spatial–temporal features in time series MSG SEVIRI images for multi-temporal cloud detection. This method allows accurate detection of clouds at either daytime or nighttime by exploiting their temporal correlation to the sequence images. Zhang et al. (2021) recently developed a multi-temporal cloud detection method (MCD-RPCA) that exploits spectral-spatial–temporal features. MCD-RPCA applies spectral threshold testing, principal component analysis, temporal change detection, and morphological processing from spectral, spectral-temporal, and spatial perspectives and achieves high-precision cloud detection in Landsat-8 images. Similarly, Wang et al. (2021) proposed a spatiotemporal integration approach (ST-ACSS) for CCS detection in PlanetScope images. ST-ACSS initially applies an adaptive threshold approach based on spectral, spatial, and temporal information to initialize the preliminary cloud/shadow masks, which are then refined via morphological processing and cloud shadow matching to produce the final masks.

Both traditional thresholding and machine learning methods have been applied in multi-temporal and mono-temporal cloud detection, thereby confirming the necessity of classifying cloud detection from both the features/data and algorithm perspectives. In general, on the basis of spectral-spatial features, the temporal change features of the sequence images further increase the information for CCS detection and thereby improve detection accuracy, especially in large areas covered by bright surfaces. Moreover, as a complement to spectral-temporal features, the utilization of spatial features further improves the spatial accuracy and continuity of cloud detection results, such as by reducing the noise in complex urban areas in CCS masks. While spectral-spatial–temporal feature combined methods maximize the use of information from the image itself, these methods have attracted limited research attention yet are deemed most promising for CCS detection in image time series.

3.5. Multi-source features

In addition to obtaining spectral-spatial–temporal information from the image itself, multi-source-feature based methods also mine auxiliary information for CCS detection from multi-source data that are spatially matched with an image. Such auxiliary data can be taken from multiple sources, such as ice/snow data (Rossow and Garder, 1993), surface temperature (Frey et al., 2008), DEMs (Huang et al., 2010), synthetic cloud-free images (Sun et al., 2016), land cover maps (Sun et al., 2018), and water occurrences (Qiu et al., 2019), which are combined with cloudy images to enrich features utilized in CCS detection and thus improve accuracy.

CCS detection methods based on multi-source data can be either simple thresholding methods or DL-based methods with unique methodological characteristics and advantages. Sun et al. (2016) developed a universal dynamic threshold cloud detection algorithm (UDTCDA) supported by a constructed MODIS monthly cloud-free reflectance database to realize cloud detection for different satellite images. Results show that UDTCDA cloud masks have less estimation uncertainty compared with MODIS cloud mask products. Given that the construction of a cloud-free reflectance database relies on high temporal resolution images, the multi-source-feature based methods supported by a prior reflectance database are more applicable to images that are acquired by geostationary satellites or satellites with short revisit intervals. Qiu et al. (2017, 2019) combined DEM and water occurrence as auxiliary data to improve the CCS detection accuracy of earlier versions of Fmask in specific situations, especially high-altitude mountains and water areas where false detection is prone to occur. On this basis, Chen et al. (2021) and Wu et al. (2021) developed the DL-based cloud detection method that combines geographical auxiliary data by mining geosemantic information from auxiliary data, including latitude, longitude, time, and height data. This method demonstrates a significantly improved cloud detection performance in cloud-snow coexistence scenarios.

Generally, multi-source-feature based methods outperform mono-temporal methods by mining additional useful information from auxiliary data. Although these methods show potential in improving CCS detection accuracy in extreme cases, the additional need for auxiliary data limits their wide application. Moreover, given that auxiliary data usually have low resolution, these methods are more suitable for low- and medium-resolution images.

4. Algorithms

Various algorithms for CCS detection have been developed, which can be broadly classified into physical-rule based, temporal-change based, variational-model based, and machine-learning based algorithms. This review categorizes CCS detection algorithms from both the feature and algorithm perspectives, because we think features and algorithms do not have a one-to-one correspondence relationship and different types of algorithms can utilize the same types of features/data and vice versa. The selected CCS detection algorithms are listed in Table 2, which also provides the input data for each algorithm. The performance of these algorithms for images of different satellites, such as Landsat (Foga et al., 2017) and Sentinel-2 (Baetens et al., 2019; Sanchez et al., 2020; Tarrio et al., 2020; Zekoll et al., 2021), has also been compared. Some open-source CCS detection tools are presented in Appendix A.

4.1. Physical-rule based algorithms

Physical-rule based‘ algorithms set rules for threshold segmentation

Table 2
Selected CCS detection algorithms for multi-source image data.

Algorithms	References	Name of algorithm	Applicable imagery (mainly)	Input data
Physical-rule based algorithms	Saunders and Kriebel, 1988; Gesell, 1989	APOLLO	AVHRR	Mono-temporal image
	Liu et al., 1995	N/A	GMS-4	Mono-temporal image, microwave satellite data
	Simpson et al., 1998	SMC	ATSR	Mono-temporal image
	Lutz, 1999	MPEF	Meteosat-6, GOES-8	Mono-temporal image
	Derrien and Le Gléau, 2005	SAFNWC	MSG SEVIRI	Mono-temporal image
	Hutchison et al., 2005	VCM	VIIRS	Mono-temporal image
	Irish et al., 2006	ACCA	Landsat-7	Mono-temporal image
	Wang and Shi, 2006	N/A	MODIS, SeaWiFS	Mono-temporal image
	Luo et al., 2008	CCRS	MODIS	Mono-temporal image
	Le Hégarat-Mascle and André, 2009	N/A	SPOT-4 HRVIR	Mono-temporal image
	Huang et al., 2010	N/A	Landsat TM/ETM+	Mono-temporal image, DEM
	Oreopoulos et al., 2011	LTK	Landsat-7	Mono-temporal image
	Scaramuzza et al., 2012	FT-ACCA/AT-ACCA	Landsat-8	Mono-temporal image
	Zhu and Woodcock, 2012	Fmask	Landsat 4–8, Sentinel-2	Mono-temporal image
	Fisher, 2013	SPOTCASM	SPOT-5 HRG	Mono-temporal image
	Braaten et al., 2015	MSScvm	Landsat 1–5 MSS	Mono-temporal image, DEM
	Sun et al., 2016	UDTCDA	MODIS, Landsat-8	Mono-temporal image, Reference reflectance
	Li et al., 2017	MFC	Gaofen-1 WFV	Mono-temporal image
	Mei et al., 2017	XBAER-CM	ENVISAT MERIS	Mono-temporal image
	Frantz et al., 2018	$Fmask_{CDI}$	Sentinel-2	Mono-temporal image
	Qiu et al., 2019	Fmask 4.0	Landsats 4–8, Sentinel-2	Mono-temporal image, DEM, Water occurrence
	Fernandez-Moran et al., 2021	N/A	Sentinel-3	Mono-temporal image, DEM
Temporal-change based algorithms	Rossow and Garder, 1993	ISCCP	Satellite infrared and visible radiances	Multi-temporal images, ice/snow data, other ancillary data
	Cayula and Cornillon, 1996	N/A	AVHRR SST	Multi-temporal images
	Jedlovec et al., 2008	BCT	GOES-12	Multi-temporal images
	Ricciardelli et al., 2008	MACSP	MSG SEVIRI	Multi-temporal images
	Lyapustin et al., 2008	MAIAC-CM	MODIS	Multi-temporal images
	Hagolle et al., 2010	MTCD	Landsat, Formosat-2	Multi-temporal images
	Jin et al., 2013	N/A	Landsat ETM+	Multi-temporal images
	Goodwin et al., 2013	N/A	Landsat	Multi-temporal images
	Liu and Liu, 2013	IBCD	MODIS	Multi-temporal images
	Zhu and Woodcock, 2014b	Tmask	Landsat images	Multi-temporal images
	Bian et al., 2016	N/A	Huanjing-1A/B CCD	Multi-temporal images
	Mateo-García et al., 2018	MCM-GEE	Landsat-8	Multi-temporal images
	Zhu and Helmer, 2018	ATSA	Landsat-4/8, Sentinel-2	Multi-temporal images
	Candra et al., 2019	MCM	Landsat-8	Multi-temporal images, DEM
	Qiu et al., 2020	Cmask	Landsat-8	Multi-temporal images
	Zhang et al., 2021	MCD-RPCA	Landsat-8	Multi-temporal images
	Wang et al., 2021	STI-ACSS	PlanetScope	Multi-temporal images
Variational-model based algorithms	Chen et al., 2019	TVLRSDC	Landsat-8, Sentinel-2	Multi-temporal images
	Duan et al., 2020	TSSTO	Gaofen-1 WFV, SPOT-5	Multi-temporal images
Machine-learning based algorithms *	Yhann and Simpson, 1995	N/A (NN based)	AVHRR	Mono-temporal image
	Ghosh et al., 2006	N/A (Fuzzy rule based)	Meteosat-5	Mono-temporal image
	Scaramuzza et al., 2012	Expanded AT-ACCA (NN based) C5 CCA (Decision tree based)	Landsat-8	Mono-temporal image
	Hughes and Hayes, 2014	SPARCS (NN based)	Landsat images	

(*continued on next page*)

Table 2 (*continued*)

Algorithms	References	Name of algorithm	Applicable imagery (mainly)	Input data
				Mono-temporal image
	Yuan and Hu, 2015	N/A (SVM based)	RapidEye, Landsat	Mono-temporal image
	Hollstein et al., 2016	cB4S2 (Bayesian based)	Sentinel-2	Mono-temporal image
	Xie et al., 2017	N/A (CNN based)	High-resolution images	Mono-temporal image
	Tuia et al., 2018	N/A (RNN based)	MSG SEVIRI	Multi-temporal images
	Li et al., 2019b	MSCFF (CNN based)	Gaofen-1, Landsat-7/8, Google Earth images	Mono-temporal image
	Wu et al., 2020	SAGAN (GAN based)	Sentinel-2	Mono-temporal image
	Li et al., 2020	WDCD (CNN based)	Gaofen-1, Ziyuan-3	Mono-temporal image
	Poulsen et al., 2020	N/A (NN based)	Sentinel-3 SLSTR	Mono-temporal image
	Chen et al., 2020a	CECD (RF based)	Landsat-8, Sentinel-2	Mono-temporal image
	Zhang et al., 2021c	CFCA-Net (CNN based)	Gaofen-1	Mono-temporal image
	Wu et al., 2021	GeoInfoNet (CNN based)	Gaofen-1	Mono-temporal image, DEM
	Li et al., 2021	CD-FM3SF (CNN based)	Sentinel-2	Mono-temporal image

* Abbreviations for machine learning algorithms. SVM: Support Vector Machine; NN: Neural Network; RF: Random Forest; CNN: Convolutional Neural Network; RNN: Recurrent Neural Network; GAN: Generative Adversarial Network.

based on the physical properties of clouds/cloud shadows to achieve their detection. These algorithms design discriminative features and determine the optimal thresholds to achieve the masking of cloud/shadow as expressed in Eq. (1). Given the presence of foreign matter in the same spectrum, accurately extracting CCS is difficult by relying only on a single spectral feature, and CCS detection can be more accurately achieved by combining multiple types of features and considering the geometric-spatial relationship between clouds and cloud shadows.

$$R > t_1 \ and/or \ R < t_2 \tag{1}$$

where R can be the designed rules based on a single band, band combination, or derived indices, etc. t_1 and t_2 are fixed/dynamic thresholds for cloud/cloud shadow segmentation.

Physical-rule based algorithms are designed according to the band settings and spectral characteristics of a particular sensor in which cloud/shadow masks can be obtained by using the multiple tests thresholding algorithm based on a single band reflectance, band ratios, and differences. The significant physical characteristics of clouds in optical satellite images include high brightness, white color, low temperature, and high elevation, whereas the significant physical characteristics of cloud shadows include low brightness and dark color (Qiu et al., 2019). In addition, given that the spectral range near 1.38 μm has significant atmospheric water vapor absorption, this range is particularly sensitive to cirrus clouds located above atmospheric water vapor and can thus be used as a cirrus channel for cirrus cloud detection (Gao et al., 1993; Qiu et al., 2020). Given that physical-rule based algorithms usually have relatively robust performance and high efficiency, they are widely used to generate official cloud mask products for assessing the quality of satellite images, such as the cloud mask algorithm (Ackerman et al., 1998; Platnick et al., 2003; Frey et al., 2008) for MODIS images, ACCA (Irish et al., 2006), and Fmask (Zhu and Woodcock, 2012; Zhu et al., 2015) for Landsat images and Sen2Cor (Sentinel-2 atmospheric correction) (Main-Knorn et al., 2017) for Sentinel-2 images. The cloud detection accuracy of these algorithms can be improved by using DEM and clean surface reflectance data as auxiliary data, such as MSScvm (Landsat MSS clear-view-mask) (Braaten et al., 2015) and UDTCDA (Sun et al., 2016). For high-resolution images with insufficient spectral information, spectral, geometric, and textural features, usually need to be combined to further improve the CCS detection results, such as MFC (Li et al., 2017). A unified spectral index and spatial matching based algorithm called CSD-SI (cloud/shadow detection based on spectral indices) was subsequently proposed for CCS detection in multispectral and hyperspectral images with parameters that need to be adjusted when applied to different types of images (Zhai et al., 2018). Particularly, Fernandez-Moran et al. (2021) took advantage of the viewing angle differences and the displacement of clouds between Sentinel-3 SLSTR nadir and oblique images to estimate cloud top heights and to accurately detect clouds and their shadows through projection.

Although the physical-rule based algorithms are widely used in practice and can achieve high CCS detection accuracy in simple scenes, such as vegetated areas, the selection of physical rules and optimal parameters in these algorithms relies on empirical determination and parameter sensitivity analysis, thereby introducing difficulties in achieving parameter adaption and global optimality, and resulting in different degrees of cloud cover estimation bias in cloud masks. In addition, the limited physical spectral information and number of feature rules lead to a lower accuracy of physical-rule based algorithms in complex scenes, such as snow/ice covered areas.

4.2. Temporal-change based algorithms

Temporal-change based algorithms achieve cloud/cloud shadow identification by detecting abrupt changes in image time series. The temporal changes in clear-sky surfaces are assumed to be relatively smooth compared with the sudden changes in surface reflectance caused by clouds/cloud shadows (Hagolle et al., 2010; Liu and Liu, 2013). Such algorithms often use synthesized or predicted cloud-free images/pixels as reference and mark areas with significant reflectivity differences from the original image as potential areas of clouds/cloud shadows, this process can be expressed as shown in Eq. (2).

$$(R - R^*) > t_1 \ and/or \ (R - R^*) < t_2 \tag{2}$$

where R and R^* are band reflectances of original images and corresponding cloud-free images, t_1 and t_2 are spectral differencing thresholds for the identification of cloud/cloud shadow.

Clear-sky image synthesis and temporal fitting are commonly used to obtain cloud-free reference data, which can be considered as approximate estimates of surface reflectance in cloud-covered areas. On the one hand, the cloud-free reference image/pixel can be acquired by selecting the most recent cloud-free image/pixel (Jin et al., 2013; Tang et al., 2013; Candra et al., 2019) and finding the minimum value in the sequence (Liu and Liu, 2013). This image/pixel is then synthesized via median filtering (Goodwin et al., 2013), predicted via linear and nonlinear regression (Gómez-Chova et al., 2017), or estimated using the low-rank matrix decomposition model (Zhang et al., 2021). The generated cloud-free reference image/pixel can then be compared pixel by pixel with the target cloud-covered image/pixel to identify clouds and their shadows in a change detection manner. On the other hand,

temporal fitting algorithms have been used for cloud detection in image time series. These algorithms include the time series model (Zhu and Woodcock, 2014b; Qiu et al., 2020), which fits the time series change trends of individual pixels in image time series based on their valid observations and achieves CCS detection by analyzing their reflectance differences from the original time series reflectance. These algorithms usually require an initial cloud/cloud shadow mask to label the validity of pixels and better fit their time series curve.

Temporal-change based algorithms are essentially multi-temporal based CCS detection algorithms that require a certain quality and quantity of input images yet show significant advantages over single-temporal algorithms, especially in image time series applications. Specifically, benefiting from the sensitivity of the temporal-change based algorithms to changes in surface reflectance due to clouds or cloud shadows, this type of algorithm has an inherent strength for the detection of thin clouds and shadows, and shows a strong ability to distinguish clouds from bright surfaces in urban areas.

4.3. Variational-model based algorithms

Variational-model based algorithms construct a variational model with a priori constraints based on the prior knowledge of CCS components in an image and the cloud-free image components. These algorithms achieve cloud detection through an optimal solution of the variational model. In general, the CCS components in an image are spatially smooth and sparse. In addition, cloud-free image time series are smooth in the temporal domain and have low-rank properties due to their strong correlation. On the basis of these characteristics, a variational model for CCS detection based on a priori information constraints can be constructed, of which a typical example is given in Eq. (3).

$$\min_{\mathscr{C},\mathscr{B}} \lambda_1 J_1(\mathscr{C}) + \lambda_2 J_2(\mathscr{B}), s.t. \mathscr{I} = \mathscr{C} + \mathscr{B}, \mathscr{B} \geq 0 \tag{3}$$

where $\mathscr{I}$ denotes the cloudy sequence images, $\mathscr{C}$ and $\mathscr{B}$ are their cloud/shadow component and cloud-free image component, J_1 and J_2 are the regularized terms which are constructed to characterize the prior knowledge of $\mathscr{C}$ and $\mathscr{B}$, including smooth, sparse, low rank, etc.

Variational-model based CCS detection algorithms have received limited research attention in recent years, and most of them implement CCS detection in the process of CCS removal at the same time. Chen et al. (2019) developed a total variation regularized low-rank sparsity decomposition model for simultaneous CCS detection and removal in multi-temporal images. This model adapts sparsity decomposition and total variation regularization to separate CCS components and guide the compensation of cloud/cloud shadow covered areas in each image. Duan et al. (2020) proposed a thick cloud removal algorithm based on the constructed temporal smoothness and sparsity regularized model, in which CCS detection can be achieved through a threshold segmentation of separated cloud/cloud shadow elements from multi-temporal images. Both these algorithms obtain binarized cloud/cloud shadow masks by thresholding decomposed CCS components, which can be acquired by optimally solving the constructed variational model.

Although the variational-model based algorithms show promise in integrated cloud detection and removal, these algorithms require input data with a certain quality and thereby may not perform well in extreme cases, such as images with continuous and heavy cloud coverage, and their specific accuracy in different scenarios needs to be further validated on a large scale. In addition, these algorithms only utilize prior knowledge in the spatial and temporal domains and ignore spectral domain information, thereby leaving room for further improvement.

4.4. Machine-learning based algorithms

Machine-learning based approaches treat image CCS detection as an image classification problem by constructing a suitable classification model and iteratively optimizing the model parameters based on large-scale training data. Therefore, the pre-trained model has the capability of CCS detection, and the interference process can be expressed in a simplified form by Eq. (4). The key to this kind of algorithm is to select representative training data, design a reasonable model architecture function, use the appropriate training strategies to optimize the model parameters, and make the model have certain generalized application capabilities.

$$Mask = F(x,\ w) \tag{4}$$

where F denotes the pre-trained classification model, x and w are the images to be processed and model parameters learned by minimizing the loss function, respectively.

Traditional machine learning algorithms, such as classical Bayesian (Hollstein et al., 2016), fuzzy clustering (Key et al., 1989; Ghosh et al., 2006; Bo et al., 2020), random forest (Ghasemian and Akhoondzadeh, 2018; Fu et al., 2019; X. Chen et al., 2020), support vector machine (SVM) (Li et al., 2015; Yuan and Hu, 2015; Ishida et al., 2018; Joshi et al., 2019), and neural network (Lee et al., 1990; Yhann and Simpson, 1995; Walder and Maclaren, 2000; Jang et al., 2006; Hughes and Hayes, 2014; Poulsen et al., 2020), have been widely used to detect CCS in different types of images. For example, Hughes and Hayes (2014) developed the spatial procedures for automated removal of cloud and shadow (SPARCS) algorithm to detect CCSs in Landsat images by training a neural network. Yuan and Hu (2015) constructed bag-of-words models based on segmented super pixels then trained SVM classifiers to distinguish cloud regions from non-cloud ones. Bai et al. (2016) and Ishida et al. (2018) combined SVM classifiers to achieve cloud detection for high-resolution satellite and MODIS images, respectively, and improved their applicability in multiple cloud detection conditions with a small number of training samples.

Machine-learning based algorithms take the spectral features of individual pixels or locally segmented regions in an image as model inputs and output category probabilities or labels that correspond to pixels or local regions. Adding spatial features to the input of the machine learning models and increasing feature diversity by introducing spatial information can also improve the CCS detection accuracy of these algorithms. Although traditional machine learning algorithms can achieve better CCS detection results with the support of sufficient training data, their ability to mine spatial features is still limited, and feature diversity cannot sufficiently cope with CCS detection in complex scenarios.

With the continuous development of machine learning technology, as a subset of machine learning, DL has witnessed significant breakthroughs in recent years and has been successfully applied in the remote sensing field (Zhu et al., 2017; Mountrakis et al., 2018; Yuan et al., 2020). Benefiting from their advantages in feature representation, DL-based algorithms have achieved the highest accuracy in image classification, and their accuracy is constantly being improved with the advancement of new techniques (Li et al., 2018). These algorithms also do not require a manual design of feature extraction and instead learn discriminative spatial and semantic features directly from training samples. The deep layers in the network significantly increase the number and diversity of features extracted by the model, thereby the classification accuracy. In recent years, DL-based algorithms have been widely used in CCS detection for optical satellite images, including CNN (Zi et al., 2018; Chai et al., 2019; Choubin et al., 2019; Ghassemi and Magli, 2019; Shendryk et al., 2019; Segal-Rozenhaimer et al., 2020; Wu et al., 2021), GAN (Zou et al., 2019; Mateo-Garcia et al., 2020; Wu et al., 2020), recurrent neural network (Tuia et al., 2018; Mateo-Garcia et al., 2019).

For example, Mateo-Garcia et al. (2017) designed a simple CNN model for cloud detection in multispectral Proba-V images and suggested that CNN has greater potential for cloud detection than classical machine learning algorithms. Xie et al. (2017) used a pre-trained CNN model to label different segmented regions based on image segmentation to detect thick clouds, thin clouds, and cloud shadows. Zhan et al.

(2017) used a CNN model to differentiate clouds from snow in satellite images. To alleviate the CCS detection problem in multi-sensor images, Li et al. (2019b) proposed a DL-based CCS detection algorithm based on multi-scale convolutional feature fusion (MSCFF), which demonstrated its applicability to multiple types of images worldwide and achieved promising results. In general, DL-based algorithms for CCS detection are applicable to different types of images, and models with different network architectures have been designed to achieve the desired results, such as Cloud-Net (Mohajerani and Saeedi, 2019) and MF-CNN (multi-scale features-CNN) (Shao et al., 2019) for Landsat images, CD-FM3SF (cloud detection method fusing multiscale spectral and spatial features) (Li et al., 2021) and KappaMask (Domnich et al., 2021) for Sentinel-2 images, WDCD (weakly supervised deep learning-based cloud detection) (Li et al., 2020), DABNet (deformable contextual and boundary weighted network) (He et al., 2021), and GeoInfoNet (geographic information driven network) (Wu et al., 2021) for Gaofen images.

Particularly, dark channel prior (Zhang et al., 2021a) and geographic information (Chen et al., 2021; Wu et al., 2021) have been introduced in DL-based CCS detection algorithms to further enhance the ability of deep models to cope with thin clouds detection and complex land covers, especially in cloud-snow coexistence areas (Chen et al., 2021; Guo et al., 2021b) wherein the advantages of DL-based algorithms are further highlighted. The use of transferring learning (Mateo-García et al., 2020) and weakly supervised learning (Zou et al., 2019; Li et al., 2020) to address the limitations of DL-based algorithms in requiring a large amount of cloud detection labeled samples has also been explored. Domain adaptation (Mateo-Garcia et al., 2020; Guo et al., 2021a) techniques have been used to reduce the labeling costs and to cope with the generalizability problem of applying deep cloud detection models for images across different sensors. Furthermore, simultaneous cloud detection and removal based on DL are also investigated (Ji et al., 2021).

Machine-learning based algorithms can achieve CCS detection away from manually designed features and learn optimal model parameters from the training data. Benefiting from the feature representation advantages of deep neural networks, machine-learning based algorithms, especially DL-based algorithms, can realize high-accuracy CCS detection and outperform other types of algorithms in complex surface scenarios, such as urban and snow/ice covered areas. However, these algorithms mostly ignore the physical properties of clouds and cloud shadows, their spatial proximity, and their geometric similarity and are heavily dependent on training data, thereby introducing serious biases in the generalized application of machine learning models when the training data are either insufficient or unrepresentative. Therefore, future DL-based CCS detection algorithms need to learn from the experiences of the physical-rule based algorithms and focus on addressing issues related to large training sample requirements and cross-sensor applications.

Literature analysis was also conducted on different types of CCS detection algorithms over different periods, the results shown in Fig. 7 confirmed that physical-rule algorithms benefiting from their simplicity and efficiency are the most popular type of CCS detection algorithms, which have been heavily studied at different periods. In addition, the results shown in Fig. 7 also indicated that DL-based methods as a branch of ML-based algorithms have gained much attention in recent years, benefiting from the great progress of DL in tasks such as image classification and the release of a large number of open-source datasets. Moreover, temporal-changes based algorithms have gradually received more attention in the past periods owing to the increase in satellite data sources and the widespread use of image time series. Notably, variational-model based algorithms have been developed in recent years, and it can be expected that such types of algorithms will have broader application potentials for integrated cloud detection and removal in multi-temporal images.

5. Validation

The validation methods of CCS algorithms are related to the type of their results, which vary along with the requirements and purpose of practical applications, and broadly include the following three types.

- ***Specific categories***: The common output of CCS detection is specific classification results, in which each pixel is assigned a specific category, for example, cloud, cloud shadow, and clear sky (Braaten et al., 2015; Li et al., 2017; Zhu and Helmer, 2018). Furthermore, the definition of categories can be highly flexible and detailed, the final output may contain cloud, haze, smoke, and clear sky when focusing on contaminations in images (Hutchison et al., 2008; Chen et al.,

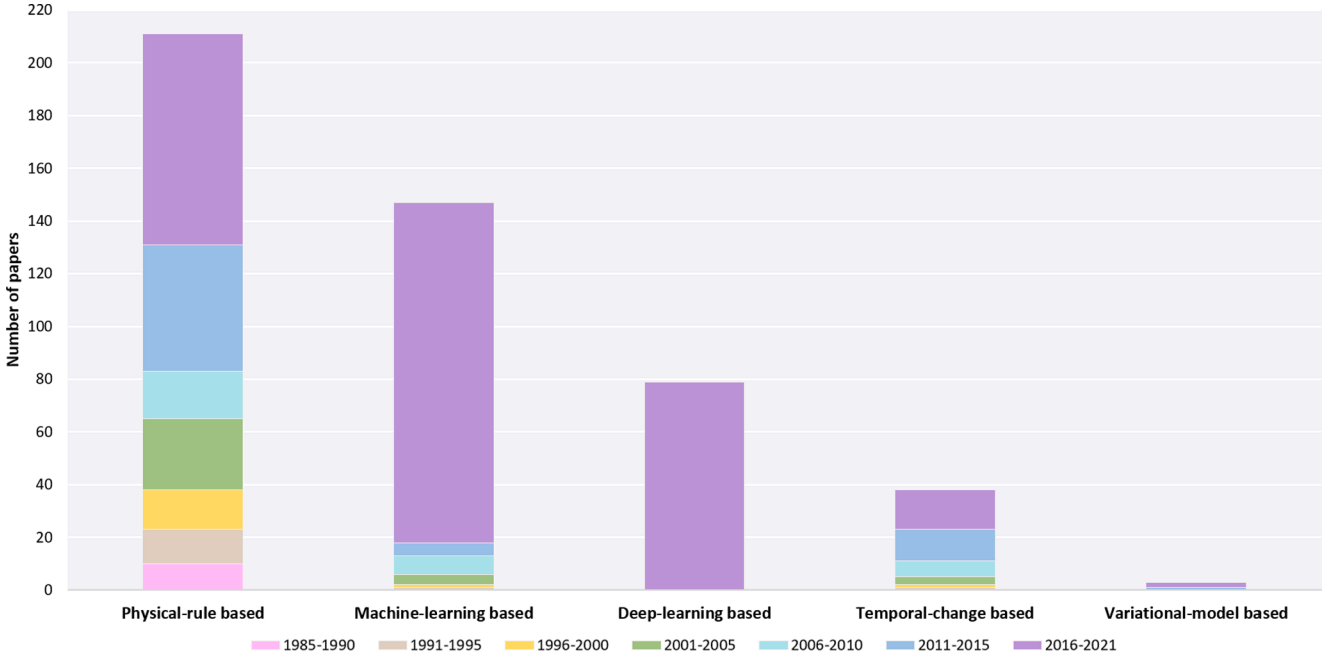

Fig. 7. Types of CCS detection algorithms developed in different periods.

2016; Zhang et al., 2019), or may contain cloud and other underlying surface types, such as vegetation, snow, and water, when concentrating on subsequent application (Luo et al., 2008; Liu and Liu, 2013).

- ***Category certainty degrees***: The CSS detection results can also be expressed in terms of the degree of category certainty, as there are uncertainties in results due to the presence of mixed pixels, especially for low-resolution images. For example, the MODIS cloud mask algorithm (Ackerman et al., 1998; Platnick et al., 2003; Frey et al., 2008) labels each pixel as one of four cloud and non-cloud certainty degrees, namely, cloud, probably cloud, probably clear, and clear. These results tend to be collections of threshold tests based on physical or statistical models (Ackerman et al., 2010; Ishida and Nakajima, 2009), in which most results are a combination of confidence levels of independent tests rather than definite classes.
- ***Cloud types***: Clouds can be classified from different perspectives, such as thickness, cloud phase, and altitude, and have infinite possibilities in terms of form, composition, and state of the location of existence (Lamb and Verlinde, 2011). In terms of cloud thickness, clouds can be simply classified into opaque and thin, with their thickness closely related to their form and location. Cloud thickness is one aspect that influences the tests deployed in cloud detection algorithms, and further research on cloud classification based on cloud phases and altitudes is specialized and closely related to nephology.

The validation of CCS detection algorithms relies on standard reference results, their accuracy can be evaluated by measuring the agreements and differences between the output and standard reference results, and the detection errors can be obtained as in general image classification methods. This review mainly focuses on the standard reference results for the algorithm quantitative validation, which broadly include four means, namely, comparing to manually labeled masks, comparing to cloud mask products, comparing to collocated LiDAR/radar data, and comparing to ground-based camera data. The selection of standard reference results for algorithm validation depends on the types of images and the availability of standard reference results.

5.1. Comparing to manually labeled masks

Comparing to manually labeled masks is a common validating algorithm for CCS detection, which draws cloud borders by visual interpretation (Li et al., 2019b), semi-automatically labeling pixels through threshold segmentation (Sun et al., 2020), computer vision annotation tools (Domnich et al., 2021), and visual checking and correction (Yu et al., 2020). CCS labels can also be obtained through cloud identification with composited low-resolution cloud-free images (Chen et al., 2020a). With the increasing interest and demand in the field of cloud detection, a growing number of open-source cloud detection datasets are being released, which contribute to the development of the field. Sample CCS detection datasets include *L7_Irish* (Scaramuzza et al., 2012; USGS., 2016a) and *L8_Biome* (Foga et al., 2017; USGS., 2016b) for Landsat images, *Sentinel-2 Cloud Mask Catalogue* (Francis et al., 2020) and *WHUS2_CD* (Li et al., 2021) for Sentinel-2 images, and *GF1_WHU* (Li et al., 2017, 2019b) and *Levir_CS* (Wu et al., 2021) for Gaofen-1 images. A manual label based validation of CCS detection results is straightforward and reliable yet requires a considerable amount of manual labor. In this review, open-source cloud detection datasets are collected as listed in Appendix B. To benefit researchers in the field of CCS detection, a project on open satellite image cloud detection resources (OpenSICDR) was launched to share the latest research outputs online (https://github.com/dr-lizhiwei/OpenSICDR).

5.2. Comparing to cloud mask products

The official cloud mask products delivered by satellite agencies have relevant high reference values for the evaluation of newly developed algorithms given that manual labels are not always available for different types of images. For example, MOD35 (MYD35 for Aqua) is a representative official cloud mask product with stable performance and relatively high accuracy in different underlying surfaces (Ackerman et al., 2010) that reports an approximately 83% agreement between MODIS and Active Remotely Sensed Cloud (ARSCL) products (Ackerman et al., 2008). The MOD35 product is proven to be reliable and satisfactory through validation with the data of four seasons and different scenarios and is considered a benchmark or standard reference cloud mask in newly developed algorithms, such as the MACSP algorithm (Ricciardelli et al., 2008). The SADIST cloud screening products for ATSR images, the CLAAS-2 dataset for MSG SEVIRI images (Drönner et al., 2018), and the NSMC cloud masks for Fengyun images (Fu et al., 2019) have also been used as reference cloud mask products for relative accuracy evaluation. Despite the convenience of evaluation algorithms based on cloud mask products, relative to the reference cloud mask products, the qualitative evaluation results obtained based on cloud mask products are not very reliable and are susceptible to the accuracy of the reference cloud mask products.

5.3. Comparing to collocated LiDAR/radar data

In addition to manual cloud labels, ground, aircraft, and satellite based LiDAR/radar observation data collocated with optical images can be used to validate cloud detection results. These data have obvious advantages and broad application prospects and are usually more convincing than official cloud mask products whose accuracy is affected by some misclassified pixels. For example, the Cloud-Aerosol Lidar with Orthogonal Polarization (CALIOP) onboard the CALIPSO satellite and the Cloud Profiling Radar (CPR) onboard CloudSat are examples for providing the LiDAR observation data that are extensively applied to validate cloud detection methods (Ackerman et al., 2008; Ricciardelli et al., 2008; Sun-Mack et al., 2010; Várnai and Marshak, 2012; Mei et al., 2017). The active laser technique provides accurate cloud layer and vertical feature information (Kittaka et al., 2011; Heidinger et al., 2016) that can be effectively used for identifying cloud pixels and thus can be used as reference cloud labels for the accurate evaluation of cloud detection methods (Liu et al., 1995; Heidinger et al., 2016; Wang et al., 2016; Poulsen et al., 2020). Nevertheless, the accuracy of cloud shadow cannot be evaluated with such means for validation. Besides, the biases in the collocation of LiDAR/radar data and optical images negatively affect the accuracy of validation, and the spatial resolution and the data coverage limitations impede the wide application of LiDAR/radar observation data in cloud detection accuracy evaluation.

5.4. Comparing to ground-based camera data

As an alternative scheme, the whole sky images acquired from ground-based cameras can be used to generate reference cloud masks for the validation of CCS detection algorithms. In the generation process, the whole sky images should be geo-referenced to optical satellite images, and then reference cloud masks can be obtained through the segmentation of the aligned whole sky images. For example, two MODIS cloud detection algorithms are evaluated based on the ground-based sky camera data derived cloud masks, which are produced using sky index and bright index (Letu et al., 2014). In addition, an experimental cloud detection dataset was created recently based on the ground-based camera data for the validation of CCS detection algorithms developed for Sentinel-2 and Landsat-8 images, in which the designed system includes cameras and automatic processing algorithms is expected to be installed at multiple sites worldwide (Skakun et al., 2021). While the validation of cloud detection algorithms using ground-based camera data reduces the time of generating a reference dataset and the subjectivity in labeling clouds, the accuracy of reference cloud masks is easily affected by the registration and cloud segmentation of whole sky images.

6. Problems and prospects

Although the current CCS detection algorithms for optical satellite images have witnessed much progress, some problems remain unsolved or need to be better resolved. This review summarizes the current problems faced in CCS detection and prospects in terms of accuracy, generalizability, efficiency, and image time series processing and applications.

6.1. Common problems and accuracy improvement for CCS detection

The results of thin cloud detection have a significant impact on the accuracy of different cloud detection algorithms. Large-area thin clouds that are similar to haze or translucent clouds in the transition region between thick clouds and the clear sky surface have large variability due to different underlying surfaces, hence impeding an accurate detection. Moreover, high bright surfaces, including snow/ice, built-up areas, and bright water bodies, can be easily misidentified in cloud detection due to their spectral properties similar to clouds, especially in areas with large-area snow/ice, given the difficulty in extracting identifiable features from the central region of large clouds and bright surfaces but with slight differences in the edge regions. Moreover, given the varying geometric characteristics of clouds in an image, the limited block size of the input image and the receptive field of the deep model, CNN-based algorithms cannot easily separate large-area clouds from non-cloud bright surfaces completely and comprehensively. To address these problems, the combination of object-oriented image analysis (OBIA) and deep models with spatial attention mechanisms and the introduction of geographical information and additional auxiliary data may benefit the detection of large-area clouds and their discrimination from snow. In addition, constructing individual models for different local scenes and learning scene adaptive models for cloud detection in different complex surfaces may also help boost accuracy.

In addition, there is still much room for improvement in cloud shadow detection. For example, the cloud shadow accuracy of the widely used Fmask algorithm for Landsat images is only about 70% (Zhu and Woodcock, 2012; Hughes and Kennedy, 2019). Cloud shadow detection has received less attention than cloud detection given that cloud shadows usually account for only a small percentage compared with clouds in images. On the one hand, cloud shadows are easily confused with dark and low-reflectivity targets in images, such as terrain shadows and water bodies, thereby challenging the accurate detection of cloud shadow, especially for high spatial resolution images in which the features of cloud shadow are not sufficiently significant. The cloud shadow detection accuracy is also limited by the accuracy of cloud detection and the errors generated by the physical-rule based models when matching clouds with their shadows. On the other hand, the overall area of cloud shadows in the image is usually much smaller than that of clouds due to the fact that most cloud shadows are obscured by clouds influenced by satellite viewing and solar angles, which may lead to sample categories imbalance and reduce the accuracy of cloud shadow detection for machine-learning based algorithms to some degree. The insufficient cloud shadow training samples in DL-based algorithms is one factor that leads to poor cloud shadow detection accuracy. In this regard, given the category imbalance between clouds and cloud shadows, introducing small sample transfer learning will help improve cloud shadow detection accuracy. Moreover, with the aid of multi-source auxiliary data (e.g., DEM), terrain shadows in images can be predicted and used to reduce the misidentification of cloud shadows.

6.2. Combination of physical model and deep learning for CCS detection and removal

Physical-rule and DL-based algorithms have been widely and individually developed for CCS detection, which can be essentially categorized as model-driven and data-driven methods given their characteristics and advantages, respectively. The model-driven (i.e. physical-rule based and variational-model based) methods are usually definite and are construed based on the empirical assumptions, which may be difficult to cope with complex land cover conditions and the solving efficiency of variational models needs to be improved. On the contrary, while the data-driven (i.e. traditional machine-learning based and DL-based) methods have more strong feature representation capabilities than model-driven methods, their performances rely heavily on training data. Considering that the acquisition of large-scale CCS training samples is time-consuming and inefficient as there are many different types of images, the combination of model-driven and data-driven methods will be promising for CCS detection, and boosting model performance and efficiency while reducing the need for training samples. In terms of features and data, the output of the physical model can be used as the prior knowledge and input features of the deep model, and the physical model such as atmospheric scattering law can also be used to stimulate cloud samples and to meet the sample requirements of the deep model to some degree. In terms of methods, model-driven (i.e. variational model) and data-driven (i.e. deep learning) methods can be combined in different forms referring to the study of Shen et al. (2021), their coupling will combine their strengths and benefit the improvements of accuracy and efficiency simultaneously. Therefore, the combination of the physical model and DL, especially the coupling of model-driven and data-driven methods, are promising for CCS detection and worths further exploration in the future.

In addition, the commonly called cloud detection usually does not include the detection of thin clouds like haze, instead, direct dehazing and thin cloud removal is performed to reduce the effect of haze and thin clouds. Considering that both haze and clouds are degrading factors affecting the quality of optical satellite images, the processing of clouds usually consists of three parts, including dehazing/thin cloud removal, cloud detection, and thick cloud removal, which are usually performed independently or partially coupled. In the future, a promising consideration is to combine physical models and data-driven methods to achieve a joint estimation of cloud thickness for both thin and thick clouds, and conduct an integrated thin/thick cloud removal to improve the image quality and usability. In particular, physical models can be used to simulate a large number of hazy and cloud-covered image samples for model training of data-driven methods, such as deep learning, to construct an integrated model for simultaneous thin and thick cloud removal in images. With the rapidly growing amount of optical satellite images, such a combination and method will be able to provide strong support for efficient cloud processing of massive images.

6.3. Development of a unified framework for CCS detection for multi-sensor images

Due to the differences in band settings and spectral responses of satellite images of different sensors, most of the current CCS detection algorithms have been developed and applied to specific types of images, thereby limiting the applicability of CCS detection algorithms for multi-sensor images. Given the increasing number of satellite image data sources, developing different algorithms for images of previously or newly launched satellites becomes inefficient. Therefore, a unified framework should be developed to boost the generalizability of CCS detection for images of multiple sensors. In this regard, analyzing common spectral characteristics and mining the invariant spatial features and even temporal difference features of images will benefit the development of a unified framework for the CCS detection of multi-sensor images. Although several recent studies have attempted to achieve multi-sensor CSS detection based on DL (Li et al., 2019b; Wieland et al., 2019), the application of current DL-based CCS detection algorithms cannot be effectively extended to other types of images due to the large sample requirements for model training and the unique characteristics of images from different sensors. With the continuous advancements of DL techniques, algorithms supported by transferring

learning techniques, such as domain adaptation, have promising applications in addressing large sample requirements, in which models trained on the source domain can also be applied to the target domain without much accuracy reduction, and thus achieve the goal of CCS detection for multi-sensor images. In addition, simulating cloudy images based on clear images of multiple sensors through advanced image synthesis techniques, such as GAN, can generate a large number of training samples with very little human effort. Such an approach can be used to meet the training requirements of multi-sensor models, and provide a new scheme for the construction of a unified framework for CCS detection in multi-sensor images.

6.4. AI-enabled online cloud processing for large-scale optical satellite data

With the release of a large amount of optical satellite data, the dense processing requirements motivate us to develop more effective online cloud detection algorithms. Online processing platforms, such as Google Earth Engine (GEE), Amazon Web Services, and Microsoft Azure, provide opportunities to quickly access and process big satellite data online to support their wide range of applications. In this case, online cloud detection algorithms are crucial to achieving a near-real-time pre-processing of optical satellite images. Recent studies (Mateo-García et al., 2018; Yin et al., 2020) have investigated cloud detection in online GEE platforms and achieved satisfactory results. In the future, the further combination of online processing platforms and artificial intelligence (AI) technologies will provide a new paradigm for the processing of large-scale satellite data, including but not limited to cloud detection, and enable the high-precision and efficient application of large-scale Earth observation data.

6.5. Integration of cloud detection/removal with image time series analysis

Image time series play an important role in the long-term monitoring of the Earth surface, however, cloud coverage causes the problem of information missing in image time series. In this regard, cloud detection and removal are both essential for the composition of clean and seamless images of desired areas, especially cloudy areas and other areas with abundant rainfall. Given that multi-temporal cloud removal usually utilizes auxiliary information from the adjacent temporal images of the same areas to reconstruct the cloud-covered areas, cloud detection and cloud removal are treated as individual processes in most previous studies. Therefore, the integrated multi-temporal cloud detection and removal will improve processing efficiency and reduce error accumulation. On the one hand, the temporal features in image time series benefit the accuracy improvement of CCS detection, especially in complex and bright land surfaces. On the other hand, image time series, which provide longer and more continuous observation information, also benefit the accurate reconstruction of cloud-covered areas. In terms of the integration of cloud detection and cloud removal, time series models (Zhu and Woodcock, 2014a, 2014b) and variational models (Chen et al., 2019; Duan et al., 2020) have demonstrated their application potentials, and more advanced techniques, such as DL, warrant further exploration.

7. Conclusions

CCS detection is an essential step in satellite image preprocessing and applications and has remained an important topic in the field of optical remote sensing. This review has examined the trends in the field through a literature survey, reviewed the CCS detection studies from the features, algorithms, and validation aspects and summarized the existing problems, and provided our prospects for future development. It can be concluded that the combination of spectral, spatial, temporal, and multi-source features from auxiliary data has been proved effective to alleviate the commission and omission problems of CCS. In terms of using only the information from the images themselves, spectral-spatial features and spectral-spatial-temporal features are the two most promising types of features that enable high-precision CCS detection. Particularly, DL-based methods have been demonstrated their superiority over other types of algorithms in CCS detection with the support of sufficient training data. Collocated LiDAR/radar data and ground-based camera data were alternative sources for validation, as the acquisition of manually labeled masks was time-consuming. Further improvement in CCS detection algorithms can be made by improving accuracy in complex conditions, and by boosting the cross-sensor generalizability by developing a unified framework. Further research is warranted in investigating the combination of physical model and deep learning, exploring the integration of thin/thick cloud detection/removal, and developing AI-enabled online processing methods for large-scale satellite data, which will facilitate efficient processing and fine applications of optical satellite imagery.

Declaration of Competing Interest

The authors declare that they have no known competing financial interests or personal relationships that could have appeared to influence the work reported in this paper.

Acknowledgments

This research was supported by the National Key Research and Development Program of China (No. 2018YFA0605500), the National Natural Science Foundation of China (No. 42101357), the China Postdoctoral Science Foundation (Nos. 2020TQ0229, 2021M692462), and the Fundamental Research Funds for the Central Universities (No. 2042021KF0078). The authors of this review would like to thank the editors and the anonymous reviewers for providing valuable comments, which helped to greatly improve the manuscript.

Appendix A:. Open-source tools for CCS detection

	Name	Applicable images (mainly)	References	Descriptions (data and method)	Link
Landsat	Fmask	Landsat 4–8 Sentinel-2	Zhu and Woodcock, 2012	Mono-temporal image Physical rule based	https://github.com/GERSL/Fmask
	Tmask	Landsat 4–8	Zhu and Woodcock, 2014b	Multi-temporal images Temporal change based	https://github.com/GERSL/Tmask
	MSScvm	Landsat MSS	Braaten et al., 2015	Multi-source data Physical rule based	https://github.com/jdbcode/MSScvm

(continued on next page)

(*continued*)

	Name	Applicable images (mainly)	References	Descriptions (data and method)	Link
	MFmask	Landsat 4–8	Qiu et al., 2017	Multi-source data Physical rule based	https://github.com/qsly09/MFmask
	MCM-GEE	Landsat-8	Mateo-García et al., 2018	Multi-temporal images Temporal change based	https://github.com/IPL-UV/ee_ipl_uv
	Cloud-Net	Landsat-8	Mohajerani and Saeedi, 2019	Mono-temporal image DL based	https://github.com/SorourMo/Cloud-Net-A-semantic-segmentation-CNN-for-cloud-detection
	Cmask	Landsat-8	Qiu et al., 2020	Multi-temporal images Temporal change based	https://github.com/GERSL/Cmask
	DAGANS	Landsat-8 Proba-V	Mateo-Garcia et al., 2020	Mono-temporal image DL based	https://github.com/IPL-UV/pvl8dagans
	FCNN	Landsats-8 Sentinel-2	López-Puigdollers et al., 2021	Mono-temporal image DL based	https://github.com/IPL-UV/DL-L8S2-UV
Sentinel-2	MAJA	Sentinel-2, VENμS, Landsat-8	Hagolle et al., 2010	Multi-temporal image Temporal change based	https://github.com/CNES/MAJA
	cB4S2	Sentinel-2	Hollstein et al., 2016	Mono-temporal image Machine learning based	https://github.com/hollstein/cB4S2
	Sen2Cor	Sentinel-2	Main-Knorn et al., 2017	Mono-temporal image Physical rule based	https://step.esa.int/main/snap-supported-plugins/sen2cor/
	s2cloudless	Sentinel-2	Zupanc, 2017	Mono-temporal image Machine learning based	https://github.com/sentinel-hub/sentinel2-cloud-detector
	FORCE	Sentinel-2 Landsat 4–8	Frantz et al., 2018	Mono-temporal image Physical rule based	https://github.com/davidfrantz/force
	KappaMask	Sentinel-2	Domnich et al., 2021	Mono-temporal image DL based	https://github.com/kappazeta/cm_predict
	CD-FM3SF	Sentinel-2	Li et al., 2021	Mono-temporal image DL based	https://github.com/Neooolee/WHUS2-CD
Gaofen	MFC	Gaofen-1 WFV	Li et al., 2017	Mono-temporal image Physical rule based	http://sendimage.whu.edu.cn/en/mfc
	GeoInfoNet	Gaofen-1 WFV	Wu et al., 2021	Mono-temporal image DL based	https://github.com/permanentCH5/GeoInfoNet
Others	N/A	HR images	Xie et al., 2017	Mono-temporal image DL based	http://xfy.buaa.edu.cn/code.html

Appendix B. Open-source datasets for CCS detection.

Name	Source	References	Descriptions	Link
L7_Irish	Landsat-7 (30 m)	Scaramuzza et al., 2012; USGS., 2016a	Contains 206 Landsat-7 scenes from nine global latitude zones with manually generated masks, of which only 45 scenes are labeled for cloud shadows.	https://landsat.usgs.gov/landsat-7-cloud-cover-assessment-validation-data
L8_SPARCS	Landsat-8 (30 m)	Hughes and Hayes, 2014;	Contains 80 subsets of Landsat-8	https://www.usgs.gov/core-science-systems/nli/landsat/spatial-procedures-automated-removal-cloud-and-shadow-sparcs

(*continued on next page*)

(*continued*)

Name	Source	References	Descriptions	Link
		USGS., 2016c	scenes with a size of 1000 × 1000 pixels that are labeled for both clouds and cloud shadows.	
L8_Biome	Landsat-8 (30 m)	Foga et al., 2017; USGS., 2016b	Contains 96 Landsat-8 scenes from eight global biomes with manually generated cloud masks, of which 32 scenes are labeled for cloud shadows.	https://landsat.usgs.gov/landsat-8-cloud-cover-assessment-validation-data
95-Cloud	Landsat-8 (30 m)	Mohajerani and Saeedi, 2019	Contains 95 Landsat-8 images and associated pixel-level cloud labels that is an extension of the previously established 38-Cloud dataset.	https://github.com/SorourMo/95-Cloud-An-Extension-to-38-Cloud-Dataset
Snow-Cloud Validation Masks	Landsat-8 (30 m)	Stillinger and Collar, 2019	Contains 13 Landsat-8 images and corresponding clouds and snow labels at mid-latitude mountainous regions.	https://zenodo.org/record/3240937
RICE_dataset	Landsat-8 (30 m)	Lin et al., 2019	Contains 450 Landsat-8 images and corresponding cloud-free images and cloud labels with a size of 512 × 512 pixels in one of two subsets of the dataset.	https://github.com/BUPTLdy/RICE_DATASET
WHU Cloud Dataset	Landsat-8 (30 m)	Ji et al., 2021	Contains 7 Landsat-8 images and corresponding cloud-free historical images and cloud and shadow masks in six different regions.	https://gpcv.whu.edu.cn/data/WHU_Cloud_Dataset.html
S2-Hollstein	Sentinel-2 (10 m)	Hollstein et al., 2016	Consists 5,647,725 pixels based on images acquired over the entire globe with cloud, cirrus, snow, shadow, and water labels.	https://git.gfz-potsdam.de/EnMAP/sentinel2_manual_classification_clouds
S2-BaetensHagolle	Sentinel-2 (10 m)		Provides cloud masks for 38	https://zenodo.org/record/1460961

(*continued on next page*)

(*continued*)

Name	Source	References	Descriptions	Link
		Baetens and Hagolle, 2018	Sentinel-2 scenes selected in 2017 or 2018, each with cloud and cloud shadow labels.	
T-S2/T-PS	Sentinel-2 (10 m) PlanetScope (3 m)	Shendryk et al., 2019	Contains 4,993 Sentinel-2 and 4,943 PlanetScope subscenes with a size of 512 × 512 pixels and only RGB and NIR bands over the Wet Tropics of Australia, each is labeled at the block level.	https://data.mendeley.com/datasets/6gdybpjnwh/1
Sentinel-2 Cloud Mask Catalogue	Sentinel-2 (10 m)	Francis et al., 2020	Comprises 20 m resolution cloud masks for 513 subscenes, of which 424 subscenes are labeled for cloud shadows.	https://zenodo.org/record/4172871
Sentinel-2 KappaZeta	Sentinel-2 (10 m)	Domnich et al., 2021	Contains 4403 labeled image blocks with a size of 512 × 512 pixels from 155 Sentinel-2 images over the Northern European terrestrial area.	https://zenodo.org/record/5095024
WHUS2-CD	Sentinel-2 (10 m)	Li et al., 2021	Contains 32 Sentinel-2 images distributed in Mainland China and its reference cloud masks labeled at 10 m resolution.	https://github.com/Neooolee/WHUS2-CD
GF1_WHU	Gaofen-1 WFV (16 m)	Li et al., 2017	Contains 108 globally distributed GF-1 WFV scenes and their manually labeled cloud and cloud shadow masks.	http://sendimage.whu.edu.cn/en/mfc-validation-data
Levir_CS	Gaofen-1 WFV (16 m)	Wu et al., 2021	Contains 4,168 globally distributed Gaofen-1 WFV scenes (down sampled to 160 m resolution) and the corresponding geographical data, cloud, and snow labels.	https://github.com/permanentCH5/GeoInfoNet
WDCD dataset	Gaofen-1 PMS	Li et al., 2020	Contains over 200,000	https://github.com/weichenrs/WDCD

(*continued on next page*)

(*continued*)

Name	Source	References	Descriptions	Link
	(8 m) Ziyuan-3 MUX (5.8 m)		globally distributed Gaofen-1 image blocks labeled at the block level for training and 30 Gaofen-1 and Ziyuan-3 scenes labeled at the pixel level for validation and testing.	
N/A	Gaofen series (N/A)	Sun et al., 2020	Contains 745 paired NIR-R-G composited images and corresponding pixel-level labels with a size of 256 × 256 pixels.	https://bhpan.buaa.edu.cn/#/link/DDC7765A5A049E0F9A0DAD0E9F7692C5
AIR-CD	Gaofen-2 PMS (4 m)	He et al., 2021	Contains 34 Gaofen-2 full images and the corresponding cloud labels distributed at different regions of China.	https://github.com/AICyberTeam/AIR-CD
HRC_WHU	Google Earth (0.5 m to 15 m)	Li et al., 2019b	Comprises 150 globally distributed high-resolution images (0.5 m to 15 m resolution, three RGB channels) and the corresponding cloud masks.	http://sendimage.whu.edu.cn/en/hrc_whu

References

Ackerman, S., Richard, F., Kathleen, S., Yinghui, L., Chris, M., Liam, G., Bryan, B., Paul, M., 2010. Discriminating clear-sky from cloud with MODIS algorithm theoretical basis document (MOD35). University of Wisconsin -, Madison.

Ackerman, S.A., Holz, R.E., Frey, R., Eloranta, E.W., Maddux, B.C., McGill, M., 2008. Cloud detection with MODIS. Part II: Validation. J. Atmos. Oceanic Technol. 25, 1073–1086. https://doi.org/10.1175/2007JTECHA1053.1.

Ackerman, S.A., Strabala, K.I., Menzel, W.P., Frey, R.A., Moeller, C.C., Gumley, L.E., 1998. Discriminating clear sky from clouds with MODIS. J. Geophys. Res. Atmos. 103, 32141–32157. https://doi.org/10.1029/1998JD200032.

Baetens, L., Desjardins, C., Hagolle, O., 2019. Validation of copernicus Sentinel-2 cloud masks obtained from MAJA, Sen2Cor, and FMask processors using reference cloud masks generated with a supervised active learning procedure. Remote Sens. 11, 1–25. https://doi.org/10.3390/rs11040433.

Baetens, L., Hagolle, O., 2018. Sentinel-2 reference cloud masks generated by an active learning method . 10.5281/zenodo.1460961.

Bai, T., Li, D., Sun, K., Chen, Y., Li, W., 2016. Cloud detection for high-resolution satellite imagery using machine learning and multi-feature fusion. Remote Sens. 8, 715. https://doi.org/10.3390/rs8090715.

Bézy, J.L., Bensi, P., Lin, C.C., Durand, Y., Hélière, F., Regan, A., Ingmann, P., Langen, J., Berger, M., Davidson, M., Rebhan, H., 2007. ESA future earth observation explorer missions. In: in: International Geoscience and Remote Sensing Symposium (IGARSS). IEEE, pp. 212–215. https://doi.org/10.1109/IGARSS.2007.4422767.

Bian, J., Li, A., Liu, Q., Huang, C., 2016. Cloud and snow discrimination for CCD images of HJ-1A/B constellation based on spectral signature and spatio-temporal context. Remote Sens. 8, 31. https://doi.org/10.3390/rs8010031.

Bo, P., Fenzhen, S., Yunshan, M., 2020. A cloud and cloud shadow detection method based on fuzzy c-means algorithm. IEEE J. Sel. Top. Appl. Earth Obs. Remote Sens. 13, 1714–1727. https://doi.org/10.1109/JSTARS.2020.2987844.

Braaten, J.D., Cohen, W.B., Yang, Z., 2015. Automated cloud and cloud shadow identification in Landsat MSS imagery for temperate ecosystems. Remote Sens. Environ. 169, 128–138. https://doi.org/10.1016/j.rse.2015.08.006.

Candra, D.S., Phinn, S., Scarth, P., 2019. Automated cloud and cloud-shadow masking for landsat 8 using multitemporal images in a variety of environments. Remote Sensing 11, 2060. https://doi.org/10.3390/rs11172060.

Cayula, J.F., Cornillon, P., 1996. Cloud detection from a sequence of SST images. Remote Sens. Environ. 55, 80–88. https://doi.org/10.1016/0034-4257(95)00199-9.

Chai, D., Newsam, S., Zhang, H.K., Qiu, Y., Huang, J., 2019. Cloud and cloud shadow detection in Landsat imagery based on deep convolutional neural networks. Remote Sens. Environ. 225, 307–316. https://doi.org/10.1016/j.rse.2019.03.007.

Chen, S., Chen, X., Chen, J., Jia, P., Cao, X., Liu, C., 2016. An Iterative Haze Optimized Transformation for Automatic Cloud/Haze Detection of Landsat Imagery. IEEE Transactions on Geoscience and Remote Sensing 54, 2682–2694. 10.1109/TGRS.2015.2504369.

Chen, X., Liu, L., Gao, Y., Zhang, X., Xie, S., 2020a. A novel classification extension-based cloud detection method for medium-resolution optical images. Remote Sens. 12 https://doi.org/10.3390/RS12152365.

Chen, Y., He, W., Yokoya, N., Huang, T.-Z.-Z., 2019. Blind cloud and cloud shadow removal of multitemporal images based on total variation regularized low-rank sparsity decomposition. ISPRS J. Photogramm. Remote Sens. 157, 93–107. https://doi.org/10.1016/j.isprsjprs.2019.09.003.

Chen, Y., Tang, L., Kan, Z., Latif, A., Yang, X., Bilal, M., Li, Q., 2020b. Cloud and cloud shadow detection based on multiscale 3D-CNN for high resolution multispectral imagery. IEEE Access 8, 16505–16516. https://doi.org/10.1109/ACCESS.2020.2967590.

Chen, Y., Weng, Q., Tang, L., Liu, Q., Fan, R., 2021. An automatic cloud detection neural network for high-resolution remote sensing imagery with cloud-snow coexistence. IEEE Geosci. Remote Sens. Lett. 1–5 https://doi.org/10.1109/LGRS.2021.3102970.
Choubin, B., Moradi, E., Golshan, M., Adamowski, J., Sajedi-Hosseini, F., Mosavi, A., 2019. An ensemble prediction of flood susceptibility using multivariate discriminant analysis, classification and regression trees, and support vector machines. Sci. Total Environ. 651, 2087–2096. https://doi.org/10.1016/j.scitotenv.2018.10.064.
Deng, C., Li, Z., Wang, W., Wang, S., Tang, L., Bovik, A.C., 2019. Cloud detection in satellite images based on natural scene statistics and gabor features. IEEE Geosci. Remote Sens. Lett. 16, 608–612. https://doi.org/10.1109/LGRS.2018.2878239.
Derrien, M., Le Gléau, H., 2005. MSG/SEVIRI cloud mask and type from SAFNWC. Int. J. Remote Sens. 26, 4707–4732. https://doi.org/10.1080/01431160500166128.
Domnich, M., Sünter, I., Trofimov, H., Wold, O., Harun, F., Kostiukhin, A., Järveoja, M., Veske, M., Tamm, T., Voormansik, K., Olesk, A., Boccia, V., Longepe, N., Cadau, E.G., 2021. KappaMask: AI-based cloudmask processor for sentinel-2. Remote Sens. 13, 4140.
Drönner, J., Korfhage, N., Egli, S., Mühling, M., Thies, B., Bendix, J., Freisleben, B., Seeger, B., 2018. Fast cloud segmentation using convolutional neural networks. Remote Sens. 10, 1–24. https://doi.org/10.3390/rs10111782.
Duan, C., Pan, J., Li, R., 2020. Thick cloud removal of remote sensing images using temporal smoothness and sparsity regularized tensor optimization. Remote Sens. 12, 3446. https://doi.org/10.3390/rs12203446.
Fernandez-Moran, R., Gómez-Chova, L., Alonso, L., Mateo-García, G., López-Puigdollers, D., 2021. Towards a novel approach for Sentinel-3 synergistic OLCI/SLSTR cloud and cloud shadow detection based on stereo cloud-top height estimation. ISPRS J. Photogramm. Remote Sens. 181, 238–253. https://doi.org/10.1016/j.isprsjprs.2021.09.013.
Fisher, A., 2013. Cloud and cloud-shadow detection in SPOT5 HRG imagery with automated morphological feature extraction. Remote Sensing 6, 776–800. https://doi.org/10.3390/rs6010776.
Foga, S., Scaramuzza, P.L., Guo, S., Zhu, Z., Dilley, R.D., Beckmann, T., Schmidt, G.L., Dwyer, J.L., Joseph Hughes, M., Laue, B., 2017. Cloud detection algorithm comparison and validation for operational Landsat data products. Remote Sens. Environ. 194, 379–390. https://doi.org/10.1016/j.rse.2017.03.026.
Francis, A., Mrziglod, J., Sidiropoulos, P., Muller, J.-P., 2020. Sentinel-2 cloud mask catalogue. Zenodo.
Frantz, D., Haß, E., Uhl, A., Stoffels, J., Hill, J., 2018. Improvement of the Fmask algorithm for Sentinel-2 images: Separating clouds from bright surfaces based on parallax effects. Remote Sens. Environ. 215, 471–481. https://doi.org/10.1016/j.rse.2018.04.046.
Frey, R.A., Ackerman, S.A., Liu, Y., Strabala, K.I., Zhang, H., Key, J.R., Wang, X., 2008. Cloud detection with MODIS. Part I: improvements in the MODIS cloud mask for collection 5. J. Atmos. Oceanic Technol. 25, 1057–1072. https://doi.org/10.1175/2008JTECHA1052.1.
Fu, H., Shen, Y., Liu, J., He, G., Chen, J., Liu, P., Qian, J., Li, J., 2019. Cloud detection for FY meteorology satellite based on ensemble thresholds and random forests approach. Remote Sensing 11, 44. https://doi.org/10.3390/rs11010044.
Gao, B.-C., Goetz, A.F.H., Wiscombe, W.J., 1993. Cirrus cloud detection from airborne imaging spectrometer data using the 1.38 μm water vapor band. Geophys. Res. Lett. https://doi.org/10.1029/93GL00106.
Gesell, G., 1989. An algorithm for snow and ice detection using AVHRR data an extension to the APOLLO software package. Int. J. Remote Sens. 10, 897–905. https://doi.org/10.1080/01431168908903929.
Ghasemian, N., Akhoondzadeh, M., 2018. Introducing two Random Forest based methods for cloud detection in remote sensing images. Adv. Space Res. 62, 288–303. https://doi.org/10.1016/j.asr.2018.04.030.
Ghassemi, S., Magli, E., 2019. Convolutional neural networks for on-board cloud screening. Remote Sens. 11, 1–14. https://doi.org/10.3390/rs11121417.
Ghosh, A., Pal, N.R., Das, J., 2006. A fuzzy rule based approach to cloud cover estimation. Remote Sens. Environ. 100, 531–549. https://doi.org/10.1016/j.rse.2005.11.005.
Giuffrida, G., Diana, L., de Gioia, F., Benelli, G., Meoni, G., Donati, M., Fanucci, L., 2020. CloudScout: a deep neural network for on-board cloud detection on hyperspectral images. Remote Sens. 12, 1–17. https://doi.org/10.3390/rs12142205.
Gómez-Chova, L., Amorós-López, J., Mateo-García, G., Muñoz-Marí, J., Camps-Valls, G., 2017. Cloud masking and removal in remote sensing image time series. J. Appl. Remote Sens. 11, 015005 https://doi.org/10.1117/1.jrs.11.015005.
Goodman, A.H., Henderson-Sellers, A., 1988. Cloud detection and analysis: a review of recent progress. Atmos. Res. 21, 203–228. https://doi.org/10.1016/0169-8095(88)90027-0.
Goodwin, N.R., Collett, L.J., Denham, R.J., Flood, N., Tindall, D., 2013. Cloud and cloud shadow screening across Queensland, Australia: an automated method for Landsat TM/ETM+ time series. Remote Sens. Environ. 134, 50–65. https://doi.org/10.1016/j.rse.2013.02.019.
Gu, X., Tong, X., 2015. Overview of China earth observation satellite programs. IEEE Geosci. Remote Sens. Mag. 3, 113–129. https://doi.org/10.1109/MGRS.2015.2467172.
Guo, H., Liu, G., Liang, D., Zhang, L., Xiao, H., 2018. Progress of earth observation and earth science in China. Chinese J. Space Sci. 38, 797–809. https://doi.org/10.11728/cjss2018.05.797.
Guo, J., Yang, J., Yue, H., Liu, X., Li, K., 2021a. Unsupervised Domain-Invariant Feature Learning for Cloud Detection of Remote Sensing Images. IEEE Transactions on Geoscience and Remote Sensing 2892, 1–1. 10.1109/tgrs.2021.3120001.
Guo, J., Yang, J., Yue, H., Tan, H., Hou, C., Li, K., 2021b. CDnetV2: CNN-based cloud detection for remote sensing imagery with cloud-snow coexistence. IEEE Trans. Geosci. Remote Sens. 59, 700–713. https://doi.org/10.1109/TGRS.2020.2991398.
Hagolle, O., Huc, M., Pascual, D.V., Dedieu, G., 2010. A multi-temporal method for cloud detection, applied to FORMOSAT-2, VENμS, LANDSAT and SENTINEL-2 images. Remote Sens. Environ. 114, 1747–1755. https://doi.org/10.1016/j.rse.2010.03.002.
Harris, R., Baumann, I., 2015. Open data policies and satellite Earth observation. Space Policy 32, 44–53. https://doi.org/10.1016/j.spacepol.2015.01.001.
Harris, R., Olby, N., 2001. Earth observation data archiving in the USA and Europe. Space Policy 17, 35–48. https://doi.org/10.1016/S0265-9646(00)00052-7.
He, Q., Sun, X., Yan, Z., Fu, K., 2021. DABNet: deformable contextual and boundary-weighted network for cloud detection in remote sensing images. IEEE Trans. Geosci. Remote Sens. 1–16 https://doi.org/10.1109/TGRS.2020.3045474.
Heidinger, A., Foster, M., Botambekov, D., Hiley, M., Walther, A., Li, Y., 2016. Using the NASA EOS A-train to probe the performance of the NOAA PATMOS-x cloud fraction CDR. Remote Sensing 8, 1–18. https://doi.org/10.3390/rs8060511.
Hollstein, A., Segl, K., Guanter, L., Brell, M., Enesco, M., 2016. Ready-to-use methods for the detection of clouds, cirrus, snow, shadow, water and clear sky pixels in Sentinel-2 MSI images. Remote Sensing 8, 1–18. https://doi.org/10.3390/rs8080666.
Hu, X., Wang, Y., Shan, J., 2015. Automatic recognition of cloud images by using visual saliency features. IEEE Geosci. Remote Sens. Lett. 12, 1760–1764. https://doi.org/10.1109/LGRS.2015.2424531.
Huang, C., Thomas, N., Goward, S.N., Masek, J.G., Zhu, Z., Townshend, J.R.G.G., Vogelmann, J.E., 2010. Automated masking of cloud and cloud shadow for forest change analysis using Landsat images. Int. J. Remote Sens. 31, 5449–5464. https://doi.org/10.1080/01431160903369642.
Huang, W., Wang, Y., Chen, X., 2018. Cloud detection for high-resolution remote-sensing images of urban areas using colour and edge features based on dual-colour models. Int. J. Remote Sens. 39, 6657–6675. https://doi.org/10.1080/01431161.2018.1466069.
Hughes, M.J., Hayes, D.J., 2014. Automated detection of cloud and cloud shadow in single-date Landsat imagery using neural networks and spatial post-processing. Remote Sens. 6, 4907–4926. https://doi.org/10.3390/rs6064907.
Hughes, M.J., Kennedy, R., 2019. High-quality cloud masking of landsat 8 imagery using convolutional neural networks. Remote Sens. 11, 2591. https://doi.org/10.3390/rs11212591.
Hutchison, K.D., Iisager, B.D., Kopp, T.J., Jackson, J.M., 2008. Distinguishing aerosols from clouds in global, multispectral satellite data with automated cloud classification algorithms. J. Atmos. Oceanic Technol. 25, 501–518. https://doi.org/10.1175/2007JTECHA1004.1.
Hutchison, K.D., Roskovensky, J.K., Jackson, J.M., Heidinger, A.K., Kopp, T.J., Pavolonis, M.J., Frey, R., 2005. Automated cloud detection and classification of data collected by the Visible Infrared Imager Radiometer Suite (VIIRS). Int. J. Remote Sens. 26, 4681–4706. https://doi.org/10.1080/01431160500196786.
Irish, R.R., Barker, J.L., Goward, S.N., Arvidson, T., 2006. Characterization of the landsat-7 ETM+ automated cloud-cover assessment (ACCA) algorithm. Photogrammetric Engineering and Remote Sensing 72, 1179–1188. 10.14358/PERS.72.10.1179.
Ishida, H., Nakajima, T.Y., 2009. Development of an unbiased cloud detection algorithm for a spaceborne multispectral imager. J. Geophys. Res. Atmos. 114 https://doi.org/10.1029/2008JD010710.
Ishida, H., Oishi, Y., Morita, K., Moriwaki, K., Nakajima, T.Y., 2018. Development of a support vector machine based cloud detection method for MODIS with the adjustability to various conditions. Remote Sens. Environ. 205, 390–407. https://doi.org/10.1016/j.rse.2017.11.003.
Jang, J.D., Viau, A.A., Anctil, F., Bartholomé, E., 2006. Neural network application for cloud detection in SPOT VEGETATION images. Int. J. Remote Sens. 27, 719–736. https://doi.org/10.1080/01431160500106892.
Jedlovec, G.J., Haines, S.L., LaFontaine, F.J., 2008. Spatial and temporal varying thresholds for cloud detection in GOES imagery. IEEE Trans. Geosci. Remote Sens. 46, 1705–1717. https://doi.org/10.1109/TGRS.2008.916208.
Ji, S., Dai, P., Lu, M., Zhang, Y., 2021. Simultaneous cloud detection and removal from bitemporal remote sensing images using cascade convolutional neural networks. IEEE Trans. Geosci. Remote Sens. 59, 732–748. https://doi.org/10.1109/TGRS.2020.2994349.
Jin, S., Homer, C., Yang, L., Xian, G., Fry, J., Danielson, P., Townsend, P.A., 2013. Automated cloud and shadow detection and filling using two-date Landsat imagery in the USA. Int. J. Remote Sens. 34, 1540–1560. https://doi.org/10.1080/01431161.2012.720045.
Joshi, P.P., Wynne, R.H., Thomas, V.A., 2019. Cloud detection algorithm using SVM with SWIR2 and tasseled cap applied to Landsat 8. Int. J. Appl. Earth Obs. Geoinf. 82, 101898 https://doi.org/10.1016/j.jag.2019.101898.
Key, J.R., Maslanik, J.A., Barry, R.G., 1989. Cloud classification from satellite data using a fuzzy sets algorithm: a polar example. Int. J. Remote Sens. 10, 1823–1842. https://doi.org/10.1080/01431168908904014.
Kittaka, C., Winker, D.M., Vaughan, M.A., Omar, A., Remer, L.A., 2011. Intercomparison of column aerosol optical depths from CALIPSO and MODIS-Aqua. Atmos. Meas. Tech. 4, 131–141. https://doi.org/10.5194/amt-4-131-2011.
Lamb, D., Verlinde, J., 2011. Physics and chemistry of clouds, Physics and Chemistry of Clouds. Cambridge University Press. 10.1017/CBO9780511976377.
Le Hégarat-Mascle, S., André, C., 2009. Use of Markov Random Fields for automatic cloud/shadow detection on high resolution optical images. ISPRS J. Photogramm. Remote Sens. 64, 351–366. https://doi.org/10.1016/j.isprsjprs.2008.12.007.
Lee, J., Weger, R.C., Sengupta, S.K., Welch, R.M., 1990. A neural network approach to cloud classification. IEEE Trans. Geosci. Remote Sens. 28, 846–855. https://doi.org/10.1109/36.58972.
Letu, H., Nagao, T.M., Nakajima, T.Y., Matsumae, Y., 2014. Method for validating cloud mask obtained from satellite measurements using ground-based sky camera. Appl. Opt. 53, 7523. https://doi.org/10.1364/ao.53.007523.

Li, J., Wu, Z., Hu, Z., Jian, C., Luo, S., Mou, L., Zhu, X.X., Molinier, M., 2021. A lightweight deep learning-based cloud detection method for Sentinel-2A imagery fusing multiscale spectral and spatial features. IEEE Trans. Geosci. Remote Sens. 1–19 https://doi.org/10.1109/TGRS.2021.3069641.

Li, P., Dong, L., Xiao, H., Xu, M., 2015. A cloud image detection method based on SVM vector machine. Neurocomputing 169, 34–42. https://doi.org/10.1016/j.neucom.2014.09.102.

Li, Y., Chen, W., Zhang, Y., Tao, C., Xiao, R., Tan, Y., 2020. Accurate cloud detection in high-resolution remote sensing imagery by weakly supervised deep learning. Remote Sens. Environ. 250 https://doi.org/10.1016/j.rse.2020.112045.

Li, Z., Shen, H., Cheng, Q., Li, W., Zhang, L., 2019a. Thick cloud removal in high-resolution satellite images using stepwise radiometric adjustment and residual correction. Remote Sens. 11, 1925. https://doi.org/10.3390/rs11161925.

Li, Z., Shen, H., Cheng, Q., Liu, Y., You, S., He, Z., 2019b. Deep learning based cloud detection for medium and high resolution remote sensing images of different sensors. ISPRS J. Photogramm. Remote Sens. 150, 197–212. https://doi.org/10.1016/j.isprsjprs.2019.02.017.

Li, Z., Shen, H., Li, H., Xia, G., Gamba, P., Zhang, L., 2017. Multi-feature combined cloud and cloud shadow detection in GaoFen-1 wide field of view imagery. Remote Sens. Environ. 191, 342–358. https://doi.org/10.1016/j.rse.2017.01.026.

Li, Z., Shen, H., Wei, Y., Cheng, Q., Yuan, Q., 2018. Cloud detection by fusing multi-scale convolutional features. ISPRS Annals of the Photogrammetry, Remote Sensing and Spatial Information Sciences 149–152. https://doi.org/10.5194/isprs-annals-IV-3-149-2018.

Lin, C.-H.-H., Lin, B.-Y.-Y., Lee, K.-Y.-Y., Chen, Y.-C.-C., 2015. Radiometric normalization and cloud detection of optical satellite images using invariant pixels. ISPRS J. Photogramm. Remote Sens. 106, 107–117. https://doi.org/10.1016/j.isprsjprs.2015.05.003.

Lin, D., Xu, G., Wang, X., Wang, Y., Sun, X., Fu, K., 2019. A Remote Sensing Image Dataset for Cloud Removal. arXiv preprint arXiv:1901.00600.

Liu, G., Curry, J.A., Sheu, R.-S., 1995. Classification of clouds over the western equatorial Pacific Ocean using combined infrared and microwave satellite data. J. Geophys. Res. 100, 811–826. https://doi.org/10.1029/95jd00823.

Liu, R., Liu, Y., 2013. Generation of new cloud masks from MODIS land surface reflectance products. Remote Sens. Environ. 133, 21–37. https://doi.org/10.1016/j.rse.2013.01.019.

López-Puigdollers, D., Mateo-García, G., Gómez-Chova, L., 2021. Benchmarking deep learning models for cloud detection in landsat-8 and sentinel-2 images. Remote Sensing 13, 1–20. https://doi.org/10.3390/rs13050992.

Luo, Y., Trishchenko, A.P., Khlopenkov, K.V., 2008. Developing clear-sky, cloud and cloud shadow mask for producing clear-sky composites at 250-meter spatial resolution for the seven MODIS land bands over Canada and North America. Remote Sens. Environ. 112, 4167–4185. https://doi.org/10.1016/j.rse.2008.06.010.

Lutz, H.-J., 1999. Cloud processing for METEOSAT Second Generation. Technical Memorandum No . 4.

Lyapustin, A.I., Wang, Y., Frey, R., 2008. An automatic cloud mask algorithm based on time series of MODIS measurements. J. Geophys. Res. Atmos. 113, 1–15. https://doi.org/10.1029/2007JD009641.

Ma, H., Liang, S., Shi, H., Zhang, Y., 2021. An optimization approach for estimating multiple land surface and atmospheric variables from the geostationary advanced himawari imager top-of-atmosphere observations. IEEE Trans. Geosci. Remote Sens. 59, 2888–2908. https://doi.org/10.1109/TGRS.2020.3007118.

Mahajan, S., Fataniya, B., 2020. Cloud detection methodologies: variants and development—a review. Compl. Intell. Syst. 6, 251–261. https://doi.org/10.1007/s40747-019-00128-0.

Main-Knorn, M., Pflug, B., Louis, J., Debaecker, V., Müller-Wilm, U., Gascon, F., 2017. Sen2Cor for Sentinel-2, in: Bruzzone, L., Bovolo, F., Benediktsson, J.A. (Eds.), Image and Signal Processing for Remote Sensing XXIII. SPIE, p. 3. 10.1117/12.2278218.

Mateo-Garcia, G., Adsuara, J.E., Perez-Suay, A., Gomez-Chova, L., 2019. Convolutional Long Short-Term Memory Network for Multitemporal Cloud Detection over Landmarks. In: International Geoscience and Remote Sensing Symposium (IGARSS). IEEE, pp. 210–213. https://doi.org/10.1109/IGARSS.2019.8897832.

Mateo-García, G., Gómez-Chova, L., Amorós-López, J., Muñoz-Marí, J., Camps-Valls, G., 2018. Multitemporal cloud masking in the Google Earth Engine. Remote Sens. 10, 7–9. https://doi.org/10.3390/rs10071079.

Mateo-Garcia, G., Gomez-Chova, L., Camps-Valls, G., 2017. Convolutional neural networks for multispectral image cloud masking. In: 2017 IEEE International Geoscience and Remote Sensing Symposium (IGARSS). IEEE, pp. 2255–2258. https://doi.org/10.1109/IGARSS.2017.8127438.

Mateo-Garcia, G., Laparra, V., Lopez-Puigdollers, D., Gomez-Chova, L., 2020. Cross-sensor adversarial domain adaptation of Landsat-8 and Proba-V images for cloud detection. IEEE J. Sel. Top. Appl. Earth Obs. Remote Sens. 14, 747–761. https://doi.org/10.1109/JSTARS.2020.3031741.

Mateo-García, G., Laparra, V., López-Puigdollers, D., Gómez-Chova, L., 2020. Transferring deep learning models for cloud detection between Landsat-8 and Proba-V. ISPRS J. Photogramm. Remote Sens. 160, 1–17. https://doi.org/10.1016/j.isprsjprs.2019.11.024.

Mei, L., Vountas, M., Gómez-Chova, L., Rozanov, V., Jäger, M., Lotz, W., Burrows, J.P., Hollmann, R., 2017. A Cloud masking algorithm for the XBAER aerosol retrieval using MERIS data. Remote Sens. Environ. 197, 141–160. https://doi.org/10.1016/j.rse.2016.11.016.

Meyer, P., Itten, K.I., Kellenberger, T., Sandmeier, S., Sandmeier, R., 1993. Radiometric corrections of topographically induced effects on Landsat TM data in an alpine environment. ISPRS J. Photogramm. Remote Sens. 48, 17–28. https://doi.org/10.1016/0924-2716(93)90028-L.

Mohajerani, S., Saeedi, P., 2019. Cloud-Net: An End-To-End Cloud Detection Algorithm for Landsat 8 Imagery. In: International Geoscience and Remote Sensing Symposium (IGARSS). IEEE, pp. 1029–1032. https://doi.org/10.1109/IGARSS.2019.8898776.

Mountrakis, G., Li, J., Lu, X., Hellwich, O., 2018. Deep learning for remotely sensed data. ISPRS J. Photogramm. Remote Sens. 145, 1–2. https://doi.org/10.1016/j.isprsjprs.2018.08.011.

Neeck, S.P., Magner, T.J., Paules, G.E., 2005. NASA's small satellite missions for Earth observation. Acta Astronaut. 56, 187–192. https://doi.org/10.1016/j.actaastro.2004.09.034.

Oreopoulos, L., Wilson, M.J., Várnai, T., 2011. Implementation on landsat data of a simple cloud-mask algorithm developed for MODIS land bands. IEEE Geosci. Remote Sens. Lett. 8, 597–601. https://doi.org/10.1109/LGRS.2010.2095409.

Platnick, S., King, M.D.M.D., Ackerman, S.A.S.A., Menzel, W.P.P., Baum, B.A.B.A., Riedi, J.C., Frey, R.A.R.A., Riédi, J.C., Frey, R.A.R.A., 2003. The MODIS cloud products: algorithms and examples from terra. IEEE Trans. Geosci. Remote Sens. 41, 459–473. https://doi.org/10.1109/TGRS.2002.808301.

Poulsen, C., Egede, U., Robbins, D., Sandeford, B., Tazi, K., Zhu, T., 2020. Evaluation and comparison of a machine learning cloud identification algorithm for the SLSTR in polar regions. Remote Sens. Environ. 248 https://doi.org/10.1016/j.rse.2020.111999.

Purkis, S.J., Klemas, V. V., 2013. Remote Sensing and Global Environmental Change, Remote Sensing and Global Environmental Change. John Wiley & Sons. 10.1002/9781118687659.

Qiu, S., He, B., Zhu, Z., Liao, Z., Quan, X., 2017. Improving Fmask cloud and cloud shadow detection in mountainous area for Landsats 4–8 images. Remote Sens. Environ. 199, 107–119. https://doi.org/10.1016/j.rse.2017.07.002.

Qiu, S., Zhu, Z., He, B., 2019. Fmask 4.0: Improved cloud and cloud shadow detection in Landsats 4–8 and Sentinel-2 imagery. Remote Sens. Environ. 231, 111205 https://doi.org/10.1016/j.rse.2019.05.024.

Qiu, S., Zhu, Z., Woodcock, C.E., 2020. Cirrus clouds that adversely affect Landsat 8 images: what are they and how to detect them? Remote Sens. Environ. 246, 111884 https://doi.org/10.1016/j.rse.2020.111884.

Ricciardelli, E., Romano, F., Cuomo, V., 2008. Physical and statistical approaches for cloud identification using meteosat second generation-spinning enhanced visible and infrared imager data. Remote Sens. Environ. 112, 2741–2760. https://doi.org/10.1016/j.rse.2008.01.015.

Rossow, W.B., Garder, L.C., 1993. Cloud detection using satellite measurements of infrared and visible radiances for ISCCP. J. Clim. https://doi.org/10.1175/1520-0442(1993)006<2341:CDUSMO>2.0.CO;2.

Sanchez, A.H., Picoli, M.C.A., Camara, G., Andrade, P.R., Chaves, M.E.D., Lechler, S., Soares, A.R., Marujo, R.F.B., Simões, R.E.O., Ferreira, K.R., Queiroz, G.R., 2020. Comparison of cloud cover detection algorithms on sentinel-2 images of the Amazon tropical forest. Remote Sens. 12, 1–16. https://doi.org/10.3390/RS12081284.

Saunders, R.W., Kriebel, K.T., 1988. An improved method for detecting clear sky and cloudy radiances from AVHRR data. Int. J. Remote Sens. 9, 123–150. https://doi.org/10.1080/01431168808954841.

Scaramuzza, P.L., Bouchard, M.A., Dwyer, J.L., 2012. Development of the landsat data continuity mission cloud-cover assessment algorithms. IEEE Transactions on Geoscience and Remote Sensing 50, 1140–1154. 10.1109/TGRS.2011.2164087.

Segal-Rozenhaimer, M., Li, A., Das, K., Chirayath, V., 2020. Cloud detection algorithm for multi-modal satellite imagery using convolutional neural-networks (CNN). Remote Sens. Environ. 237, 111446 https://doi.org/10.1016/j.rse.2019.111446.

Shao, Z., Pan, Y., Diao, C., Cai, J., 2019. Cloud detection in remote sensing images based on multiscale features-convolutional neural network. IEEE Trans. Geosci. Remote Sens. 57, 4062–4076. https://doi.org/10.1109/TGRS.2018.2889677.

Shen, H., Li, X., Cheng, Q., Zeng, C., Yang, G., Li, H., Zhang, L., 2015. Missing information reconstruction of remote sensing data: a technical review. IEEE Geosci. Remote Sens. Mag. 3, 61–85. https://doi.org/10.1109/MGRS.2015.2441912.

Shen, H., Member, S., Jiang, M., Li, J., Zhou, C., 2021. Coupling Model-Driven and Data-Driven Methods for Remote Sensing Image Restoration and Fusion. arXiv preprint arXiv:2108.06073 1–15.

Shendryk, Y., Rist, Y., Ticehurst, C., Thorburn, P., 2019. Deep learning for multi-modal classification of cloud, shadow and land cover scenes in PlanetScope and Sentinel-2 imagery. ISPRS J. Photogramm. Remote Sens. 157, 124–136. https://doi.org/10.1016/j.isprsjprs.2019.08.018.

Shimada, M., 2014. JAXA earth observation programs digest. IEEE Geosci. Remote Sens. Mag. 2, 47–52. https://doi.org/10.1109/mgrs.2014.2318308.

Simpson, J.J., Jin, Z., Stitt, J.R., 2000. Cloud shadow detection under arbitrary viewing and illumination conditions. IEEE Trans. Geosci. Remote Sens. 38, 972–976. https://doi.org/10.1109/36.841979.

Simpson, J.J., Schmidt, A., Harris, A., 1998. Improved cloud detection in along track scanning radiometer (ATSR) data over the ocean. Remote Sens. Environ. 65, 1–24. https://doi.org/10.1016/S0034-4257(98)00025-X.

Simpson, J.J., Stitt, J.R., 1998. A procedure for the detection and removal of cloud shadow from AVHRR data over land. IEEE Trans. Geosci. Remote Sens. 36, 880–897. https://doi.org/10.1109/36.673680.

Skakun, S., Vermote, E.F., Artigas, A.E.S., Rountree, W.H., Roger, J.C., 2021. An experimental sky-image-derived cloud validation dataset for Sentinel-2 and Landsat 8 satellites over NASA GSFC. Int. J. Appl. Earth Obs. Geoinf. 95, 102253 https://doi.org/10.1016/j.jag.2020.102253.

Stillinger, T., Collar, N., 2019. Snow-Cloud Validation Masks for Multispectral Satellite Data [Data set]. 10.5281/zennodo.3240937.

Sun-Mack, S., Minnis, P., Kato, S., Chen, Y., Yi, Y., Gibson, S., Heck, P., Winker, D., Ayers, K., 2010. Enhanced cloud algorithm from collocated CALIPSO, CloudSat and MODIS global boundary layer lapse rate studies. In: International Geoscience and

Remote Sensing Symposium (IGARSS). IEEE, pp. 201–204. https://doi.org/10.1109/IGARSS.2010.5649624.
Sun, H., Li, L., Xu, M., Li, Q., Huang, Z., 2020. Using minimum component and CNN for satellite remote sensing image cloud detection. IEEE Geosci. Remote Sens. Lett. 1–5 https://doi.org/10.1109/LGRS.2020.3014358.
Sun, L., Mi, X., Wei, J., Wang, J., Tian, X., Yu, H., Gan, P., 2017. A cloud detection algorithm-generating method for remote sensing data at visible to short-wave infrared wavelengths. ISPRS J. Photogramm. Remote Sens. 124, 70–88. https://doi.org/10.1016/j.isprsjprs.2016.12.005.
Sun, L., Wei, J., Wang, J., Mi, X., Guo, Y., Lv, Y., Yang, Y., Gan, P., Zhou, X., Jia, C., Tian, X., 2016. A universal dynamic threshold cloud detection algorithm (UDTCDA) supported by a prior surface reflectance database. J. Geophys. Res. 121, 7172–7196. https://doi.org/10.1002/2015JD024722.
Sun, L., Zhou, X., Wei, J., Wang, Q., Liu, X., Shu, M., Chen, T., Chi, Y., Zhang, W., 2018. A new cloud detection method supported by GlobeLand30 Data Set. IEEE J. Sel. Top. Appl. Earth Obs. Remote Sens. 11, 3624–3645. https://doi.org/10.1109/JSTARS.2018.2861755.
Tang, H., Yu, K., Hagolle, O., Jiang, K., Geng, X., Zhao, Y., 2013. A cloud detection method based on a time series of MODIS surface reflectance images. Int. J. Digital Earth 6, 157–171. https://doi.org/10.1080/17538947.2013.833313.
Tapakis, R., Charalambides, A.G., 2013. Equipment and methodologies for cloud detection and classification: a review. Sol. Energy 95, 392–430. https://doi.org/10.1016/j.solener.2012.11.015.
Tarrio, K., Tang, X., Masek, J.G., Claverie, M., Ju, J., Qiu, S., Zhu, Z., Woodcock, C.E., 2020. Comparison of cloud detection algorithms for Sentinel-2 imagery. Sci. Remote Sens. 2, 100010 https://doi.org/10.1016/j.srs.2020.100010.
Tuia, D., Kellenberger, B., Perez-Suey, A., Camps-Valls, G., 2018. A Deep Network Approach to Multitemporal Cloud Detection, in. In: IGARSS 2018–2018 IEEE International Geoscience and Remote Sensing Symposium. IEEE, pp. 4351–4354. https://doi.org/10.1109/IGARSS.2018.8517312.
USGS., 2016a. L7 Irish Cloud Validation Masks. U.S. Geological Survey data release. https://landsat.usgs.gov/landsat-7-cloud-cover-assessment-validation-data.
USGS., 2016b. L8 Biome Cloud Validation Masks. U.S. Geological Survey, data release. https://landsat.usgs.gov/landsat-8-cloud-cover-assessment-validation-data.
USGS., 2016c. L8 SPARCS Cloud Validation Masks. U.S. Geological Survey data release. https://www.usgs.gov/core-science-systems/nli/landsat/spatial-procedures-automated-removal-cloud-and-shadow-sparcs.
Várnai, T., Marshak, A., 2012. Analysis of co-located MODIS and CALIPSO observations near clouds. Atmos. Meas. Tech. 5, 389–396. https://doi.org/10.5194/amt-5-389-2012.
Walder, P., Maclaren, I., 2000. Neural network based methods for cloud classification on AVHRR images. Int. J. Remote Sens. 21, 1693–1708. https://doi.org/10.1080/014311600209977.
Wang, J., Yang, D., Chen, S., Zhu, X., Wu, S., Bogonovich, M., Guo, Z., Zhu, Z., Wu, J., 2021. Automatic cloud and cloud shadow detection in tropical areas for PlanetScope satellite images. Remote Sens. Environ. 264, 112604 https://doi.org/10.1016/j.rse.2021.112604.
Wang, M., Shi, W., 2006. Cloud masking for ocean color data processing in the coastal regions. IEEE Trans. Geosci. Remote Sens. 44, 3196–3205. https://doi.org/10.1109/TGRS.2006.876293.
Wang, T., Fetzer, E.J., Wong, S., Kahn, B.H., Yue, Q., 2016. Validation of MODIS cloud mask and multilayer flag using CloudSat-CALIPSO cloud profiles and a cross-reference of their cloud classifications. J. Geophys. Res. 121, 11620–11635. https://doi.org/10.1002/2016JD025239.
Wieland, M., Li, Y., Martinis, S., 2019. Multi-sensor cloud and cloud shadow segmentation with a convolutional neural network. Remote Sens. Environ. 230, 111203 https://doi.org/10.1016/j.rse.2019.05.022.
Wu, X., Shi, Z., 2018. Utilizing multilevel features for cloud detection on satellite imagery. Remote Sensing 10, 1–23. https://doi.org/10.3390/rs10111853.
Wu, X., Shi, Z., Zou, Z., 2021. A geographic information-driven method and a new large scale dataset for remote sensing cloud/snow detection. ISPRS J. Photogramm. Remote Sens. 174, 87–104. https://doi.org/10.1016/j.isprsjprs.2021.01.023.
Wu, Z., Li, J., Wang, Y., Hu, Z., Molinier, M., 2020. Self-attentive generative adversarial network for cloud detection in high resolution remote sensing images. IEEE Geosci. Remote Sens. Lett. 17, 1792–1796. https://doi.org/10.1109/LGRS.2019.2955071.
Wulder, M.A., Coops, N.C., 2014. Satellites: Make Earth observations open access. Nature 513, 30–31. https://doi.org/10.1038/513030a.
Xie, F., Shi, M., Shi, Z., Yin, J., Zhao, D., 2017. Multilevel cloud detection in remote sensing images based on deep learning. IEEE J. Sel. Top. Appl. Earth Obs. Remote Sens. 10, 3631–3640. https://doi.org/10.1109/JSTARS.2017.2686488.
Yang, J., Guo, J., Yue, H., Liu, Z., Hu, H., Li, K., 2019. CDnet: CNN-based cloud detection for remote sensing imagery. IEEE Trans. Geosci. Remote Sens. 57, 6195–6211. https://doi.org/10.1109/TGRS.2019.2904868.
Yhann, S.R., Simpson, J.J., 1995. Application of neural networks to AVHRR cloud segmentation. IEEE Trans. Geosci. Remote Sens. 33, 590–604. https://doi.org/10.1109/36.387575.
Yin, Z., Ling, F., Foody, G.M., Li, X., Du, Y., 2020. Cloud detection in Landsat-8 imagery in Google Earth Engine based on a deep convolutional neural network. Remote Sens. Lett. 11, 1181–1190. https://doi.org/10.1080/2150704X.2020.1833096.
Yu, J., Li, Y., Zheng, X., Zhong, Y., He, P., 2020. An effective cloud detection method for gaofen-5 images via deep learning. Remote Sens. 12, 2106. https://doi.org/10.3390/rs12132106.
Yuan, Q., Shen, H., Li, T., Li, Z., Li, S., Jiang, Y., Xu, H., Tan, W., Yang, Q., Wang, J., Gao, J., Zhang, L., 2020. Deep learning in environmental remote sensing: achievements and challenges. Remote Sens. Environ. 241, 111716 https://doi.org/10.1016/j.rse.2020.111716.
Yuan, Y., Hu, X., 2015. Bag-of-words and object-based classification for cloud extraction from satellite imagery. IEEE J. Sel. Top. Appl. Earth Obs. Remote Sens. 8, 4197–4205. https://doi.org/10.1109/JSTARS.2015.2431676.
Zekoll, V., Main-Knorn, M., Louis, J., Frantz, D., Richter, R., Pflug, B., 2021. Comparison of masking algorithms for sentinel-2 imagery. Remote Sens. 13, 1–21. https://doi.org/10.3390/rs13010137.
Zhai, H., Zhang, H., Zhang, L., Li, P., 2018. Cloud/shadow detection based on spectral indices for multi/hyperspectral optical remote sensing imagery. ISPRS J. Photogramm. Remote Sens. 144, 235–253. https://doi.org/10.1016/j.isprsjprs.2018.07.006.
Zhan, Y., Wang, J., Shi, J., Cheng, G., Yao, L., Sun, W., 2017. Distinguishing cloud and snow in satellite images via deep convolutional network. IEEE Geosci. Remote Sens. Lett. 14, 1785–1789. https://doi.org/10.1109/LGRS.2017.2735801.
Zhang, H., Huang, Q., Zhai, H., Zhang, L., 2021. Multi-temporal cloud detection based on robust PCA for optical remote sensing imagery. Comput. Electron. Agric. 188, 106342 https://doi.org/10.1016/j.compag.2021.106342.
Zhang, J., Wang, H., Wang, Y., Zhou, Q., Li, Y., 2021a. Deep network based on up and down blocks using wavelet transform and successive multi-scale spatial attention for cloud detection. Remote Sens. Environ. 261, 112483 https://doi.org/10.1016/j.rse.2021.112483.
Zhang, J., Wu, J., Wang, H., Wang, Y., Li, Y., 2021c. Cloud detection method using CNN based on cascaded feature attention and channel attention. IEEE Trans. Geosci. Remote Sens. 1–1 https://doi.org/10.1109/tgrs.2021.3120752.
Zhang, Q., Yuan, Q., Li, Z., Sun, F., Zhang, L., 2021d. Combined deep prior with low-rank tensor SVD for thick cloud removal in multitemporal images. ISPRS J. Photogramm. Remote Sens. 177, 161–173. https://doi.org/10.1016/j.isprsjprs.2021.04.021.
Zhang, X., Tan, S.C., Shi, G.Y., Wang, H., 2019. Improvement of MODIS cloud mask over severe polluted eastern China. Sci. Total Environ. 654, 345–355. https://doi.org/10.1016/j.scitotenv.2018.10.369.
Zhang, Y., Guindon, B., Cihlar, J., 2002. An image transform to characterize and compensate for spatial variations in thin cloud contamination of Landsat images. Remote Sens. Environ. 82, 173–187. https://doi.org/10.1016/S0034-4257(02)00034-2.
Zhang, Y., Guindon, B., Li, X., 2014. A robust approach for object-based detection and radiometric characterization of cloud shadow using haze optimized transformation. IEEE Trans. Geosci. Remote Sens. 52, 5540–5547. https://doi.org/10.1109/TGRS.2013.2290237.
Zhang, Y., Rossow, W.B., Lacis, A.A., Oinas, V., Mishchenko, M.I., 2004. Calculation of radiative fluxes from the surface to top of atmosphere based on ISCCP and other global data sets: refinements of the radiative transfer model and the input data. J. Geophys. Res.: Atmos. 109, D19105. https://doi.org/10.1029/2003JD004457.
Zhu, X., Helmer, E.H., 2018. An automatic method for screening clouds and cloud shadows in optical satellite image time series in cloudy regions. Remote Sens. Environ. 214, 135–153. https://doi.org/10.1016/j.rse.2018.05.024.
Zhu, X.X., Tuia, D., Mou, L., Xia, G.-S., Zhang, L., Xu, F., Fraundorfer, F., 2017. Deep Learning in remote sensing: a comprehensive review and list of resources. IEEE Geosci. Remote Sens. Mag. 5, 8–36. https://doi.org/10.1109/MGRS.2017.2762307.
Zhu, Z., Qiu, S., He, B., Deng, C., 2019a. Cloud and cloud shadow detection for landsat images: the fundamental basis for analyzing landsat time series. Remote Sens. Time Series Image Process. 3–23 https://doi.org/10.1201/9781315166636-1.
Zhu, Z., Wang, S., Woodcock, C.E., 2015. Improvement and expansion of the Fmask algorithm: Cloud, cloud shadow, and snow detection for Landsats 4–7, 8, and Sentinel 2 images. Remote Sens. Environ. 159, 269–277. https://doi.org/10.1016/j.rse.2014.12.014.
Zhu, Z., Woodcock, C.E., 2014a. Continuous change detection and classification of land cover using all available Landsat data. Remote Sens. Environ. 144, 152–171. https://doi.org/10.1016/j.rse.2014.01.011.
Zhu, Z., Woodcock, C.E., 2014b. Automated cloud, cloud shadow, and snow detection in multitemporal Landsat data: an algorithm designed specifically for monitoring land cover change. Remote Sens. Environ. 152, 217–234. https://doi.org/10.1016/j.rse.2014.06.012.
Zhu, Z., Woodcock, C.E., 2012. Object-based cloud and cloud shadow detection in Landsat imagery. Remote Sens. Environ. 118, 83–94. https://doi.org/10.1016/j.rse.2011.10.028.
Zhu, Z., Wulder, M.A., Roy, D.P., Woodcock, C.E., Hansen, M.C., Radeloff, V.C., Healey, S.P., Schaaf, C., Hostert, P., Strobl, P., Pekel, J.F., Lymburner, L., Pahlevan, N., Scambos, T.A., 2019b. Benefits of the free and open Landsat data policy. Remote Sens. Environ. 224, 382–385. https://doi.org/10.1016/j.rse.2019.02.016.
Zi, Y., Xie, F., Jiang, Z., 2018. A cloud detection method for Landsat 8 images based on PCANet. Remote Sens. 10, 1–21. https://doi.org/10.3390/rs10060877.
Zou, Z., Li, W., Shi, T., Shi, Z., Ye, J., 2019. Generative adversarial training for weakly supervised cloud matting. In: Proceedings of the IEEE International Conference on Computer Vision. IEEE, pp. 201–210. https://doi.org/10.1109/ICCV.2019.00029.
Zupanc, A., 2017. Improving cloud detection with machine learning. https://medium.com/sentinel-hub/improving-cloud-detection-with-machine-learning-c09dc5d7cf13.